Facile synthesis of tetrahedral Ag_3PO_4 mesocrystals and its enhanced photocatalytic activity

Pengyu Dong[1]*, Yao Yin[2], Ning Xu[1], Rongfeng Guan[1], Guihua Hou[1], and Yuhua Wang[3]

[1]*Key Laboratory for Advanced Technology in Environmental Protection of Jiangsu Province, Yancheng Institute of Technology, Yancheng 224051, P. R. China*

[2]*School of Civil and Environmental Engineering, Nanyang Technological University, 50 Nanyang Avenue, Singapore 639798*

[3]*Department of Materials Science, School of Physical Science and Technology, Lanzhou University, Lanzhou 730000, P. R. China*

*Corresponding author.

Tel.: +86-515-88298923 (Office), +86-18351484051(Mobile)

E-mail address: dongpy11@gmail.com

Abstract

A novel and rapid strategy has been developed to synthesize tetrahedral Ag_3PO_4 mesocrystals with the help of surfactant oleic acid. Homogeneous Ag_3PO_4 tetrahedron with average apex-to-apex length of 1.1 μm could be synthesized under optimized conditions. Oleic acid is considered to be essential for the formation of this homogeneous tetrahedral morphology. The as-prepared tetrahedral Ag_3PO_4 mesocrystals could be formed through the close-packed assembly of Ag_3PO_4 nanoparticles, thus the formation of tetrahedral Ag_3PO_4 mesocrystals is explained by the oriented aggregation mechanism based on time-dependent experiments. Furthermore, the obtained tetrahedral Ag_3PO_4 mesocrystals exhibit enhanced visible-light photocatalytic degradation of methylene blue (MB) and methyl orange (MO) solutions compared to the reported micro-sized spherical Ag_3PO_4 particles with high photocatalytic performance.

Keywords: A. Inorganic compounds; A. Semiconductors; B. Chemical synthesis; D. Catalytic properties.

1. Introduction

Photocatalysis is generally considered as a promising application technology in the fields of air cleaning and water purification [1]. The conventional TiO_2 photocatalyst has gained much attention since it possesses good activity and stability, low lost, and nontoxicity [2, 3]. However, TiO_2 has a large band gap that requires the high-energy ultraviolet (UV) light to excite, which only counts for a small fraction (3–5%) of the total solar spectrum. Although some modification technologies were explored to extend the light absorption of TiO_2 to visible light region [4-10], the present achievements are still far from the practical application. Therefore, much effort has been directed toward the development of new visible-light active photocatalysts.

In particular in the year 2010, Yi et al. reported a novel Ag_3PO_4 photocatalyst which showed extremely high photooxidative capabilities for water-splitting and organic dye decomposition under visible-light irradiation [11]. They also demonstrated that the photocatalytic activity of micro-sized spherical Ag_3PO_4 particles was superior to the traditional visible-light active photocatalysts such as N-doped TiO_2 and $BiVO_4$ [11]. The research findings are considered as a breakthrough in the field of visible-light active photocatalysts [12]. Therefore, it is urgent to further investigate the basic principles and application of Ag_3PO_4 photocatalyst in detail. So far, various methods have been proposed to further enhance the photocatalytic activity of Ag_3PO_4 under visible light irradiation. One approach is the coupling of Ag_3PO_4 with other semiconductors or noble metals to promote the charge separation efficiency of Ag_3PO_4, and thus improving the

photocatalytic activity. Some coupled systems such as Ag_3PO_4/TiO_2 [13], Ag_3PO_4/AgX (X=Cl, Br, I) [14], Ag_3PO_4/SnO_2 [15], Fe_3O_4/Ag_3PO_4 [16], Ag_3PO_4/Ag [17, 18], Ag_3PO_4/BiOCl [19], Ag_3PO_4/reduced graphite oxide sheets [20], and carbon quantum dots/Ag_3PO_4 [21] composites have recently been developed to improve the photocatalytic activity of Ag_3PO_4. Another approach is the synthesis of Ag_3PO_4 with various new morphologies. This is because photocatalytic reactions are typically surface-based processes, thus the photocatalytic efficiency is closely related to the morphology and micro-structure of a photocatalyst [22]. Recently, research on Ag_3PO_4 crystals with new morphologies and structures has drawn a great deal of attention [23-31]. For examples, Bi et al. reported the single-crystalline Ag_3PO_4 rhombic dodecahedrons with only {110} facets exposed and cubes bounded entirely by {100} facets, and they found that both of these samples exhibited higher photocatalytic activity than the micro-sized spherical Ag_3PO_4 particles [23]. Wang et al. reported the synthesis of Ag_3PO_4 tetrapod microcrystals with exposed {110} facets, and they demonstrated that Ag_3PO_4 tetrapod showed higher photocatalytic activity than the micro-sized spherical Ag_3PO_4 particles [25]. Bi's group and Xie's group reported the synthesis of tetrahedral Ag_3PO_4 structures exposed with {111} planes, respectively [29, 30]. Our former work reported the synthesis of Ag_3PO_4 crystals with various new morphologies (branch, tetrapod, nanorod, triangular prism) by adjusting external experimental conditions [31]. However, it should be noted that the reported Ag_3PO_4 samples mostly possess regular crystal structures and exposed special planes. To the best of our knowledge, there is very little research on the

fabrication of mesocrystal Ag_3PO_4. Mesocrystals are colloidal crystals composed of individual nanocrystals that are aligned in a common crystallographic fashion, exhibiting scattering properties similar to a single crystal [32]. It is known that the mesocrystalline materials received significant research attentions because they simultaneously own both high porosity and high crystallinity [32-35], which is beneficial for photocatalytic application. Thus, the controlled synthesis of Ag_3PO_4 mesocrystals is of great value.

In this work, **tetrahedral Ag_3PO_4 mesocrystals were synthesized by a new method.** The effects of synthesis conditions on morphologies are investigated in detail, and the formation mechanism of tetrahedral Ag_3PO_4 mesocrystals is proposed. It is considered that the obtained tetrahedron could be formed through the oriented self-assembly of Ag_3PO_4 nanoparticles. More importantly, the as-prepared tetrahedral Ag_3PO_4 mesocrystals exhibit excellent photocatalytic activity under visible light irradiation for methylene blue (MB) and methyl orange (MO) removal.

2. Experimental

2.1 Sample preparation

In a typical preparation procedure for tetrahedral Ag_3PO_4 mesocrystals at optimized condition, firstly, 1.4 mL oleic acid was added into 9 mL of N,N-dimethylformamide (DMF) with stirring for 10 min to form transparent solution A. Then, 1 mmol of $AgNO_3$ was added into 1 mL of deionized water (H_2O) to form transparent solution B. The total volume of mixture solvent is kept constant to 10 mL. Subsequently, solution B was added into solution A under stirring. After stirring for 10 min, H_3PO_4 (3 mL, 85%) dissolved in

5 mL of ethanol was then added dropwise into the above solution under stirring. This process needs about 15 min. The mixture was stirred for 1 h and separated by centrifuge followed by washing with ethanol and deionized water for 3 times, respectively, to remove the oleic acid, DMF, and other residues. The product was then dried in a vacuum oven at 60 °C. Other samples were prepared by the similar procedure, except for different amount of oleic acid, P source, ratio of DMF to H_2O, and reaction temperature. For comparison purpose, micro-sized spherical Ag_3PO_4 particles were synthesized by a reported method [11].

2.2 Characterization

X-ray diffraction (XRD) experiments were carried out with a D/max-2400 diffractometer (Rigaku, Tokyo, Japan) using Cu-Ka radiation. The morphologies of the samples were examined by scanning electron microscopy (SEM; S-4800, Hitachi, Tokyo, Japan). A FEI Tecnai G2 F30 (Eindhoven, the Netherlands) transmission electron microscope, equipped with a Gatan imaging filter (GIF) system, was used for transmission electron microscopy (TEM), selected-area electron diffraction pattern (SAED), and energy dispersive X-ray spectra (EDX) work. Fourier transform infrared spectrum (FTIR) of the sample was recorded between 400 and 4000 cm^{-1} on a Nicolet NEXUS 670 FTIR spectrometer (Thermo-Nicolet, Madison, WI). Ultraviolet–visible diffuse reflectance spectra (UV–vis DRS) were measured using a Perkin Elmer 950 spectrometer (Perkin Elmer, Norwalk, CT), while $BaSO_4$ was used as a reference. Specific surface areas were computed from the isotherms by applying the

Brunauer–Emmett–Teller (BET) method using a Micromeritics ASAP 2000 system (Atlanta, GA).

2.3 Evaluation of photocatalytic activity

The photocatalytic activity of samples was measured by the decomposition of MB and MO in a reactor at room temperature. In a typical process for degradation of MB and MO, the used amount of photocatalyst was 0.02 g/70 mL of MB or MO solutions (10 mg/L). Before irradiation, the suspensions were stirred in the dark for 1 h to ensure the establishment of adsorption–desorption equilibrium. A 350 W Xe lamp with a cutoff filter of 420 nm was employed for the visible-light irradiation source and positioned 20 cm away from the reactor to trigger the photocatalytic reaction. A certain volume of suspension was withdrawn at selected times for analysis. After recovering the photocatalyst by centrifugation, the concentration of dye solution was analyzed by measuring the light absorption of the clear solution at 664 nm (λ_{max} for MB solution) or 465 nm (λ_{max} for MO solution) using a spectrophotometer (WFJ-7200, Unico, USA). The percentage of degradation was calculated by C/C_0. Here, C is the concentration of remaining dye solution at each irradiated time interval, while C_0 is the initial concentration.

To compare the photocatalytic stability of spherical Ag_3PO_4 particles and tetrahedral Ag_3PO_4 mesocrystals, the cycling runs in photocatalytic degradation of MB were checked. After one cycle, the photocatalyst was filtrated and washed thoroughly with deionized water, and then fresh MB solution (10 mg/L) was added

to the photocatalyst to begin the next cycling run. Four consecutive cycles were completed and each cycle lasted for 180 min.

3. Results and Discussion

3.1 Characterizations of tetrahedral Ag_3PO_4 mesocrystals

Based on the investigation of effects of synthesis conditions on the morphologies (see Fig. S1–S4 in the Supplementary Data), it is suggested that homogeneous tetrahedral Ag_3PO_4 could be synthesized under the optimized conditions: 1.4 ml of oleic acid as the surfactant, H_3PO_4 as the phosphorus (P) source, DMF/H_2O = 9:1, room temperature, and reaction time of 1 h. Low magnification SEM image (Fig. 1a) of the resulting Ag_3PO_4 synthesized at optimized condition shows that the product mainly consists of regularly shaped tetrahedrons (accounts for 85%). The average apex-to-apex length of these tetrahedrons is taken from statistics analysis, which is about 1.1 μm, as shown in Fig. 1b. A large magnification SEM image of as-prepared Ag_3PO_4 is displayed in Fig. 1c. It is noted that the surfaces of Ag_3PO_4 tetrahedrons are not smooth enough, which are covered by many nanoparticles. In addition, it is observed that some pores exist on the surfaces of Ag_3PO_4 tetrahedron (Fig. 1d), indicating the existence of surface porous characteristics. These observations suggest that the Ag_3PO_4 tetrahedron consists of nanoparticles.

Further investigation of Ag_3PO_4 tetrahedron was carried out by TEM technology, as shown in Fig. 2a. It exhibits a triangular morphology in two dimensions that could arise from a tetrahedral morphology in three dimensions. Moreover, it is observed that many nanoparticles are attached to the edges of Ag_3PO_4 tetrahedron, which is consistent with

the SEM result. Fig. 2b displays the SAED pattern of a single Ag_3PO_4 tetrahedron. The pattern consists of diffraction spots, revealing the single-crystalline nature of each Ag_3PO_4 tetrahedron. Generally, the mesoporous structure and the "single-crystal-like" diffraction are considered as the characterizations of mesocrystalline materials [36]. Combining the above results, it can be concluded that the as-prepared sample should be tetrahedral Ag_3PO_4 mesocrystals. Fig. 2c displays the EDX spectrum of tetrahedral Ag_3PO_4 sample. It reveals the O, P, and Ag peaks except for C and Cu peaks coming from the film on the TEM grid. This result clearly confirms the existence of the O, P and Ag elements.

The phase purity of as-obtained tetrahedral product was examined by means of XRD and FTIR methods. Fig. 3a clearly reveals that all of the diffraction peaks of the as-prepared tetrahedral sample can be indexed to the body-centered cubic structure of Ag_3PO_4 (JCPDS Card No. 06-0505). Moreover, the sharp diffraction peaks indicate high crystallinity of tetrahedral Ag_3PO_4 mesocrystals. In addition, it is noted that the intensity ratios of diffraction peaks are close to that of the standard values for powder sample, suggesting there is no obvious preferred orientation behavior. Fig. 3b shows the FTIR spectrum of tetrahedral Ag_3PO_4 sample. It reveals four major absorption bands: a strong and broad absorption around 3400 cm^{-1} and a sharp band at 1670 cm^{-1} are observed, which could be attributed to the stretching vibration of O–H and the bending vibration of H–O–H of water molecules, respectively. Two strong absorption bands are observed at 989 and 558 cm^{-1}, which can be assigned to the molecular vibrations of phosphate (PO_4^{3-})

[26, 37]. This result clearly confirms that there are no oleic acid and DMF molecules adsorbed on the surface of the as-obtained tetrahedral Ag_3PO_4 sample.

3.2 Formation mechanism of tetrahedral Ag_3PO_4 mesocrystals

Reaction time-dependent experiments were carried out to investigate the formation mechanism of tetrahedral Ag_3PO_4 mesocrystals. From Fig. 4a, it is obvious that the obtained samples prepared with various reaction times all show the cubic phase of Ag_3PO_4, and the crystallinity undergoes no obvious change when prolonging the reaction time. Reaction time-dependent morphological evolution is displayed in Fig. 4b–d. At the initial stage (0 min), nanoscale Ag_3PO_4 particles with size of about 100 nm are observed (Fig. 4b). As the reaction time increased to 30 min, besides the independent nanoparticles, tetrahedral morphology is observed (Fig. 4c). It can be seen that the tetrahedron consists of a large number of nanoparticles (marked with circles in Fig. 4c). When the reaction time was prolonged to 1 h, as shown in Fig. 4d, homogeneous and regular tetrahedrons were obtained, and the independent nanoparticles disappeared, implying that the tetrahedrons could be formed by an assembly process of nanoparticles. This result agrees well with the typical formation processes of mesocrystalline materials [32], further confirming the formation of tetrahedral Ag_3PO_4 mesocrystals.

From the characterization and time-dependent morphological evolution results, it is reasonable to presume that the tetrahedral Ag_3PO_4 mesocrystals were formed through the close-packed assembly of Ag_3PO_4 nanoparticles. This pathway is in stark contrast to the classical crystallization, which usually proceeds by molecule or ion-by-ion attachment

[36]. The formation of as-obtained tetrahedral Ag_3PO_4 mesocrystals could be based on the oriented aggregation mechanism, and the formation and evolution process can be divided into three steps: the initial formation of $[Ag(amide)(solvent)]^+$ ligand complex, the nucleation and growth processes, and the subsequent self-assembly process (oriented aggregation). A schematic diagram of the proposed formation process is shown in Scheme 1. In the first stage, the silver ions (Ag^+), amide (DMF), and solvent (H_2O) could form the weakly bound $[Ag(amide)(solvent)]^+$ ligand complex [38]. In addition, the oleic acid molecules could exist around the DMF instead of H_2O molecules due to its hydrophobic property. In this stage, the ratio of DMF to H_2O affects the resulting morphology. H_2O molecules could reduce the strength of the amide-silver ion binding energy, and excess amount of H_2O could induce the amide-silver ligand bond breaking [38], thus the role of oleic acid in the control of resulting morphology is limited because oleic acid molecules exist around the DMF instead of H_2O molecules. On the other hand, as displayed in Fig. S1 (in the Supplementary Data), oleic acid is essential for the formation of tetrahedral morphology. Hence, tetrahedral morphology disappears when the samples synthesized with low DMF/H_2O ratios (excess amount of H_2O), as shown in Fig. S2 (in the Supplementary Data). In the second stage, Ag_3PO_4 crystal nucleations were carried out after H_3PO_4 was added [31]. In this process, oleic acid molecules could adsorb on the surfaces of crystal nucleuses, which could control the reaction rate and avoid the crystallographic fusion of the primary crystals to a single crystal through the oriented-attachment mechanism [39]. These nucleation clusters were grown and then

transformed to crystalline primary Ag_3PO_4 nanoparticles (as building blocks) [40]. Thus, in a very short time, stabilized Ag_3PO_4 nanoparticles with surfactant coatings were formed. The obtained nanoparticles can be regarded as "spherical core-shell nanoparticles" with an inorganic core and an organic surfactant shell. It is known that the pH value affects the adsorption of surfactant molecules at the surface of inorganics, and thus influences the morphology of samples [41, 42]. Our experimental results (Fig. S3 in the Supplementary Data) confirmed that the acidic condition is beneficial for the formation of tetrahedral Ag_3PO_4 morphology, which could be due to the strong adsorption of oleic acid molecules on the surfaces of Ag_3PO_4 crystal nucleuses under acidic condition. In addition, the influence of reaction temperature on the adsorption of surfactant molecules at the surfaces of Ag_3PO_4 crystal nucleuses cannot be ignored in this stage. When the reaction was carried out at low temperature (e.g. 0 °C, shown in Fig. S4 in the Supplementary Data), the reactant diffusion decreased considerably and the adsorption of oleic acid molecules on the surfaces of Ag_3PO_4 crystal nucleuses became difficult, which led to the uncontrollable reaction process, thus forming the micro-sized spherical particles. In the third stage, tetrahedral Ag_3PO_4 mesocrystals were formed via a self-assembly process by aggregation of the building blocks (primary Ag_3PO_4 nanoparticles). When two building blocks with adsorbed surfactant oleic acid come together, the capillary forces between them facilitate the solvent removal and strengthen the agglomeration through van der Waals attractive forces [43, 44]. At this stage, the hydrophobic interactions between surfactant oleic acid molecules are regarded as the

driving force for the assembly. After self-assembly process, the surfactant oleic acid molecules were removed by washing in ethanol for several times. Due to the stacking defects and polydispersity of nanoparticles in the self-assembly process, **some pores appeared on the surfaces of Ag_3PO_4 tetrahedron**, as displayed in Fig. 1d. It is well-known that the detailed formation mechanism for self-assembly process is still largely unclear [36]. From our experimental results, it is confirmed that the ability of oleic acid is the driving force behind these polycrystalline tetrahedral assemblies. However, why the oleic acid induces the tetrahedral instead of other polyhedral assemblies is still unknown.

3.3 Optical absorption property and photocatalytic performance

For comparison purpose, micro-sized spherical Ag_3PO_4 particles were prepared by the reported method [11] (shown in Fig. S5 in the Supplementary Data). Then, the optical absorption properties of spherical Ag_3PO_4 particles and tetrahedral Ag_3PO_4 mesocrystals were compared, as shown in Fig. 5. Generally, the absorption edges of as-prepared samples are used to characterize their optical absorption properties, which could eliminate the influence of base absorption lines [31]. The absorption edge position was determined by the intersection of baseline with tangent line of the UV–vis absorption spectrum [24, 45, 46]. From Fig. 5, it is found that the spherical Ag_3PO_4 and tetrahedral Ag_3PO_4 mesocrystals posses the same absorption edge, which is around 525 nm.

The N_2 adsorption–desorption isotherms of spherical Ag_3PO_4 particles and tetrahedral Ag_3PO_4 mesocrystals are presented in Fig. 6. It can be seen that the

areas of hysteresis loops for tetrahedral Ag_3PO_4 mesocrystals are much larger than that for spherical Ag_3PO_4 particles, which indicates that much porous structures are presented in the sample of tetrahedral Ag_3PO_4 mesocrystals. The BET analysis shows that the specific surface areas of spherical Ag_3PO_4 and tetrahedral Ag_3PO_4 mesocrystals are 1.02 and 4.65 m^2/g, respectively. This result clearly indicates that tetrahedral Ag_3PO_4 mesocrystals exhibit higher BET surface area. The inset of Fig. 6 shows the corresponding pore size distributions of these two samples. It is observed that tetrahedral Ag_3PO_4 mesocrystals show a peak around 50 nm, which could be attributed to the pores on the surfaces of Ag_3PO_4 tetrahedron (as shown in Fig. 1d). On the contrary, there is no peaks of pore size distributions for the sample of spherical Ag_3PO_4 particles.

Before the photocatalytic reaction, the sample suspension was stirred for 1 h in the dark to reach the adsorption–desorption equilibrium. The adsorption–desorption equilibriums of MB and MO dyes are shown in Fig. S6 (in the Supplementary Data). It is found that the tetrahedral Ag_3PO_4 mesocrystals exhibit higher adsorption ability than spherical Ag_3PO_4, which is consistent with the BET specific surface areas of samples. Higher BET specific surface area of tetrahedral Ag_3PO_4 mesocrystals increases the adsorption of dye molecules. The photocatalytic behaviors of spherical Ag_3PO_4 and tetrahedral Ag_3PO_4 mesocrystals were explored for degradation of the positively charged MB and negatively charged MO molecules under visible light irradiation after the adsorption–desorption equilibriums, as shown in Fig. **7**a–b. It should be pointed out that

the self-degradation of MB and MO is slight, indicating the stabilization of these two dyes under visible light irradiation. For the degradation of MB, about 97% and 72% of the initial MB molecules were decomposed by tetrahedral Ag_3PO_4 mesocrystals and spherical Ag_3PO_4 after photocatalytic reaction, respectively. Clearly, the photocatalytic degradation rate of tetrahedral Ag_3PO_4 mesocrystals is higher (25%) than that of spherical Ag_3PO_4 for the positively charged MB molecules. For the degradation of MO, about 92% of the initial MO molecules were decomposed for tetrahedral Ag_3PO_4 mesocrystals while 60% for spherical Ag_3PO_4 after photocatalytic reaction. This result indicates that tetrahedral Ag_3PO_4 mesocrystals show much higher (32%) photocatalytic degradation rate than spherical Ag_3PO_4 for the negatively charged MO molecules. Overall, the tetrahedral Ag_3PO_4 mesocrystals exhibit higher photocatalytic activity than spherical Ag_3PO_4 for degradation of MB and MO. The insets of Fig. **7**a–b display the color changes of MB and MO solution during the photocatalytic degradation process corresponding to tetrahedral Ag_3PO_4 mesocrystals. It is clear that MB and MO solutions were almost decolorized completely after the photocatalytic reactions.

The kinetics of photocatalytic reactions can be described using a first order reaction for low concentration of dye (MB and MO) solutions [47, 48]:

$$\ln(C_0 / C) = kt \quad (1)$$

where C_0 and C are the initial concentration and remaining concentration of dye solution, respectively, k is the apparent reaction rate constant, and t is the irradiation time.

Fig. **7**c–d displays the apparent rate constants (k, min^{-1}), which is determined from the slopes of ln(C_0/C) versus irradiation time. It can be seen that the apparent rate constants are 0.014 min^{-1} for tetrahedral Ag_3PO_4 mesocrystals and 0.008 min^{-1} for spherical Ag_3PO_4 during the decomposition of MB. In comparison, the apparent rate constants are 0.0098 min^{-1} for tetrahedral Ag_3PO_4 mesocrystals and 0.0036 min^{-1} for spherical Ag_3PO_4 during the decomposition of MO. Remarkably, the photocatalytic rate constants of tetrahedral Ag_3PO_4 mesocrystals are 1.8 and 2.7 times of that of spherical Ag_3PO_4 for degradation of MB and MO dye solutions, respectively. The correlation coefficient (R^2) represents the correlation degree between practical photocatalytic reaction and linear fit. It is found that the R^2 values of as-prepared samples are above 0.9, suggesting the data fit the first kinetic model well.

The reason of higher photocatalytic activity for tetrahedral Ag_3PO_4 mesocrystals could be attributed to the mesocrystal structure. The tetrahedral Ag_3PO_4 mesocrystals simultaneously possess both porous characteristics and high crystallinity. On one hand, the porous characteristics of tetrahedral Ag_3PO_4 mesocrystals contribute to a higher BET specific surface area. Since photocatalytic reactions are typically surface-based processes, the photocatalytic efficiency is closely related to the adsorption property of dyes on the surfaces of photocatalysts. The stronger the adsorption of dyes on the photocatalyst surface, the easier and faster the photocatalytic process [22]. The higher BET specific surface area of tetrahedral Ag_3PO_4 mesocrystals facilitates the adsorption of dye molecules, as shown in Fig. S6, which contributed to the higher photocatalytic activity.

On the other hand, the tetrahedral Ag_3PO_4 mesocrystals display higher crystallinity compared with spherical Ag_3PO_4 sample, as shown in Fig. S7 (in the Supplementary Data). The well-crystallized phase of tetrahedral Ag_3PO_4 mesocrystals could facilitate the transfer of photoinduced electrons during photocatalytic reactions, which decreased the probability of recombination with photoinduced holes and thus enhanced the efficiency of photocatalysis [49]. In addition, the optical absorption property is generally considered as an important factor affecting photocatalytic activity. However, it is found that the as-prepared spherical and tetrahedral Ag_3PO_4 products reveal the same absorption edge (shown in Fig. 5), implying that the light absorption property is not the major factor affecting photocatalytic activity.

Fig. 8 shows the photocatalytic stability of tetrahedral Ag_3PO_4 mesocrystals and spherical Ag_3PO_4 particles. It is observed that the photocatalytic activity of tetrahedral Ag_3PO_4 mesocrystals is decreased slowly in four successive experimental runs. However, the rate of MB degradation for spherical Ag_3PO_4 particles decreases more significantly in four successive experimental runs under the same conditions. This result indicates that the photocatalytic activity of tetrahedral Ag_3PO_4 mesocrystals is more stable compared with that of spherical Ag_3PO_4 particles.

4. Conclusion

Tetrahedral Ag_3PO_4 mesocrystals were firstly synthesized by a novel one-step chemical precipitation approach in the mixture solvent of DMF and H_2O using oleic acid as the surfactant. The homogeneous tetrahedral Ag_3PO_4 mesocrystals could be

synthesized under optimized conditions. The as-prepared tetrahedral Ag_3PO_4 mesocrystals could be formed through the close-packed assembly of Ag_3PO_4 nanoparticles based on the oriented aggregation mechanism. Oleic acid is considered as the aggregation-orienting agent for the formation of this unique Ag_3PO_4 tetrahedron. Furthermore, the photocatalytic rate constants of tetrahedral Ag_3PO_4 mesocrystals are 1.8 and 2.7 times of that of spherical Ag_3PO_4 for degradation of MB and MO dye solutions, respectively. Overall, this work shows that it is possible to design and synthesize mesocrystalline materials by a simple oleic acid-mediated approach in the mixture solvent.

Acknowledgements

This work is financially supported by the National Natural Science Foundation of China (Grant No. 21403184), Natural Science Foundation of the Jiangsu Higher Education Institutions of China (Grant No. 14KJB150025), National Key Technology R&D Program of China (Grant No. 2013BAC13B01), and National Natural Science Foundation of China (No. 21276220).

References

[1] M.R. Hoffmann, S.T. Martin, W. Choi, D.W. Bahnemann, Chem. Rev. 95 (1995) 69-96.

[2] A. Fujishima, K. Honda, Nature 238 (1972) 37-38.

[3] C.H. Cho, D.K. Kim, D.H. Kim, J. Am. Ceram. Soc. 86 (2003) 1138-1145.

[4] R. Asahi, T. Morikawa, T. Ohwaki, K. Aoki, Y. Taga, Science 293 (2001) 269-271.

[5] G. Chen, Y. Wang, J. Zhang, C. Wu, H. Liang, H. Yang, J. Nanosci. Nanotechnol. 12 (2012) 3799-3805.

[6] P. Dong, Y. Wang, L. Guo, B. Liu, S. Xin, J. Zhang, Y. Shi, W. Zeng, S. Yin, Nanoscale 4 (2012) 4641-4649.

[7] Y. Wang, G. Chen, Q. Shen, F. Zhang, G. Chen, Mater. Lett. 116 (2014) 27-30.

[8] G. Chen, Y. Wang, F. Zhang, H. Liang, F. Wang, L. Li, J. Sol-Gel Sci. Technol. 64 (2012) 564-570.

[9] P. Dong, B. Liu, Y. Wang, H. Pei, S. Yin, J. Mater. Res. 25 (2010) 2392.

[10] Y. Wang, G. Chen, Q. Shen, H. Yang, L. Li, Y. Song, J. Nanosci. Nanotechnol. 14 (2014) 4988-4994.

[11] Z. Yi, J. Ye, N. Kikugawa, T. Kako, S. Ouyang, H. Stuart-Williams, H. Yang, J. Cao, W. Luo, Z. Li, Nat. Mater. 9 (2010) 559-564.

[12] C.T. Dinh, T.D. Nguyen, F. Kleitz, T.O. Do, Chem. Commun. 47 (2011) 7797-7799.

[13] W. Yao, B. Zhang, C. Huang, C. Ma, X. Song, Q. Xu, J. Mater. Chem. 22 (2012) 4050–4055.

[14] Y. Bi, S. Ouyang, J. Cao, J. Ye, Phys. Chem. Chem. Phys. 13 (2011) 10071-10075.

[15] L. Zhang, H. Zhang, H. Huang, New J. Chem. 36 (2012) 1541–1544.

[16] G. Li, L. Mao, RSC Adv. 2 (2012) 5108–5111.

[17] Y. Bi, H. Hu, S. Ouyang, Z. Jiao, G. Lu, J. Ye, J. Mater. Chem. 22 (2012) 14847-14850.

[18] Y. Bi, H. Hu, S. Ouyang, Z. Jiao, G. Lu, J. Ye, Chem. Eur. J. 18 (2012) 14272-14275.

[19] B. Cao, P. Dong, S. Cao, Y. Wang, J. Am. Ceram. Soc. 96 (2013) 544-548.

[20] P. Dong, Y. Wang, B. Cao, S. Xin, L. Guo, J. Zhang, F. Li, Appl. Catal., B 132-133 (2013) 45-53.

[21] H. Zhang, H. Huang, H. Ming, L. Zhang, J. Mater. Chem. 22 (2012) 10501-10506.

[22] H. Tong, S. Ouyang, Y. Bi, N. Umezawa, M. Oshikiri, J. Ye, Adv. Mater. 24 (2012) 229-251.

[23] Y. Bi, S. Ouyang, N. Umezawa, J. Cao, J. Ye, J. Am. Chem. Soc. 133 (2011) 6490-6492.

[24] W. Jun, F. Teng, M. Chen, CrystEngComm 15 (2013) 39-42.

[25] H. Wang, L. He, L. Wang, P. Hu, L. Guo, X. Han, J. Li, CrystEngComm 14 (2012) 8342–8344.

[26] Q. Liang, W. Ma, Y. Shi, Z. Li, X. Yang, CrystEngComm 14 (2012) 2966-2973.

[27] Y. Bi, H. Hu, Z. Jiao, H. Yu, G. Lu, J. Ye, Phys. Chem. Chem. Phys. 14 (2012) 14486-14488.

[28] Z. Jiao, Y. Zhang, H. Yu, G. Lu, J. Ye, Y. Bi, Chem. Commun. 49 (2013) 636-638.

[29] H. Hu, Z. Jiao, H. Yu, G. Lu, J. Ye, Y. Bi, J. Mater. Chem. A 1 (2013) 2387-2390.

[30] B. Zheng, X. Wang, C. Liu, K. Tan, Z. Xie, L. Zheng, J. Mater. Chem. A 1 (2013) 12635-12640.

[31] P. Dong, Y. Wang, H. Li, H. Li, X. Ma, L. Han, J. Mater. Chem. A 1 (2013) 4651-4656.

[32] M. Niederberger, H. Colfen, Phys. Chem. Chem. Phys. 8 (2006) 3271-3287.

[33] L. Li, C.-y. Liu, CrystEngComm 12 (2010) 2073-2078.

[34] Y. Aoyama, Y. Oaki, R. Ise, H. Imai, CrystEngComm 14 (2012) 1405-1411.

[35] Z. Hong, M. Wei, T. Lan, L. Jiang, G. Cao, Energy Environ. Sci. 5 (2012) 5408-5413.

[36] H. Cölfen, M. Antonietti, Angew. Chem. Int. Ed. 44 (2005) 5576-5591.

[37] M. Thomas, S.K. Ghosh, K.C. George, Mater. Lett. 56 (2002) 386-392.

[38] V. Romanov, C.-K. Siu, U.H. Verkerk, A.C. Hopkinson, K.W.M. Siu, J. Phys. Chem. A 114 (2010) 6964-6971.

[39] Q. Gong, X. Qian, X. Ma, Z. Zhu, Cryst. Growth Des. 6 (2006) 1821-1825.

[40] H. Cölfen, S. Mann, Angew. Chem. Int. Ed. 42 (2003) 2350-2365.

[41] J. Drelich, Y. Lu, L. Chen, J.D. Miller, S. Guruswamy, Appl. Surf. Sci. 125 (1998) 236-244.

[42] L. Qi, H. Cölfen, M. Antonietti, Chem. Mater. 12 (2000) 2392-2403.

[43] V.N. Manoharan, D.J. Pine, MRS Bull. 29 (2004) 91-95.

[44] V.N.T.K. Satyanarayana, S.K. Ajay, S. Sudipta, Nanotechnology 18 (2007) 075303.

[45] A. Wolberg, J.F. Roth, J. Catal. 15 (1969) 250-255.

[46] C.-F. Chi, H.-W. Cho, H. Teng, C.-Y. Chuang, Y.-M. Chang, Y.-J. Hsu, Y.-L. Lee, Appl. Phys. Lett. 98 (2011) 012101-012101-012103.

[47] J.M. Herrmann, H. Tahiri, Y. Ait-Ichou, G. Lassaletta, A. Gonzalez-Elipe, A. Fernandez, Appl. Catal., B 13 (1997) 219-228.

[48] X.H. Wang, J.G. Li, H. Kamiyama, Y. Moriyoshi, T. Ishigaki, J. Phys. Chem. B 110 (2006) 6804-6809.

[49] H. Li, J. Li, Y. Huo, J. Phys. Chem. B 110 (2006) 1559-1565.

Figure captions:

Fig. 1. (a) SEM image of Ag_3PO_4 tetrahedron synthesized at optimized condition: 1.4 mL oleic acid, H_3PO_4, DMF/H_2O = 9:1, 25°C, 1 h; (b) the apex-to-apex length distribution of these tetrahedrons; and (c–d) Ag_3PO_4 tetrahedron at large magnifications.

Fig. 2. (a) TEM image of Ag_3PO_4 tetrahedron synthesized at optimized condition, the inset is a typical Ag_3PO_4 tetrahedron; (b) SAED pattern of a single Ag_3PO_4 tetrahedron; and (c) EDX spectrum of Ag_3PO_4 tetrahedron.

Fig. 3. XRD pattern (a) and FTIR spectrum (b) of the as-prepared tetrahedral sample.

Fig. 4. XRD patterns (a) and SEM images (b–d) of Ag_3PO_4 products prepared with various reaction times: (b) 0 min, (c) 30 min, and (d) 1 h. (1.4 mL oleic acid, H_3PO_4, DMF/H_2O = 9:1, 25 °C)

Fig. 5. UV–vis absorption spectra of spherical Ag_3PO_4 and tetrahedral Ag_3PO_4 mesocrystals.

Fig. 6. N_2 adsorption-desorption isotherms for spherical Ag_3PO_4 particles and tetrahedral Ag_3PO_4 mesocrystals. The inset is the BJH pore size distributions from N_2 desorption branch.

Fig. 7. Variation of MB (a) and MO (b) concentration against irradiation time in the presence of spherical Ag_3PO_4, tetrahedral Ag_3PO_4 mesocrystals and without photocatalyst in the dark and under visible light irradiation (the insets shows the color changes of MB

and MO solution during the photocatalytic degradation process corresponding to the tetrahedral Ag_3PO_4 mesocrystals); plots of ln(C_0/C) versus irradiation time for MB (c) and MO (d) representing the fit using a pseudo-first-order reaction rate.

Fig. 8. Repeated photocatalytic degradation of MB solution in the presence of spherical Ag_3PO_4 particles and tetrahedral Ag_3PO_4 mesocrystals under visible light irradiation.

Scheme caption:

Scheme 1. Schematic illustration of the formation of tetrahedral Ag_3PO_4 mesocrystals.

Facile synthesis of tetrahedral Ag_3PO_4 mesocrystals and its enhanced photocatalytic activity

Pengyu Dong[1]*, Yao Yin[2], Ning Xu[1], Rongfeng Guan[1], Guihua Hou[1], and Yuhua Wang[3]

[1]*Key Laboratory for Advanced Technology in Environmental Protection of Jiangsu Province, Yancheng Institute of Technology, Yancheng 224051, P. R. China*

[2]*School of Civil and Environmental Engineering, Nanyang Technological University, 50 Nanyang Avenue, Singapore 639798*

[3]*Department of Materials Science, School of Physical Science and Technology, Lanzhou University, Lanzhou 730000, P. R. China*

*Corresponding author.

Tel.: +86-515-88298923 (Office), +86-18351484051(Mobile)

E-mail address: dongpy11@gmail.com

Abstract

A novel and rapid strategy has been developed to synthesize tetrahedral Ag_3PO_4 mesocrystals with the help of surfactant oleic acid. Homogeneous Ag_3PO_4 tetrahedron with average apex-to-apex length of 1.1 μm could be synthesized under optimized conditions. Oleic acid is considered to be essential for the formation of this homogeneous tetrahedral morphology. The as-prepared tetrahedral Ag_3PO_4 mesocrystals could be formed through the close-packed assembly of Ag_3PO_4 nanoparticles, thus the formation of tetrahedral Ag_3PO_4 mesocrystals is explained by the oriented aggregation mechanism based on time-dependent experiments. Furthermore, the obtained tetrahedral Ag_3PO_4 mesocrystals exhibit enhanced visible-light photocatalytic degradation of methylene blue (MB) and methyl orange (MO) solutions compared to the reported micro-sized spherical Ag_3PO_4 particles with high photocatalytic performance.

Keywords: A. Inorganic compounds; A. Semiconductors; B. Chemical synthesis; D. Catalytic properties.

1. Introduction

Photocatalysis is generally considered as a promising application technology in the fields of air cleaning and water purification [1]. The conventional TiO_2 photocatalyst has gained much attention since it possesses good activity and stability, low lost, and nontoxicity [2, 3]. However, TiO_2 has a large band gap that requires the high-energy ultraviolet (UV) light to excite, which only counts for a small fraction (3–5%) of the total solar spectrum. Although some modification technologies were explored to extend the light absorption of TiO_2 to visible light region [4-10], the present achievements are still far from the practical application. Therefore, much effort has been directed toward the development of new visible-light active photocatalysts.

In particular in the year 2010, Yi et al. reported a novel Ag_3PO_4 photocatalyst which showed extremely high photooxidative capabilities for water-splitting and organic dye decomposition under visible-light irradiation [11]. They also demonstrated that the photocatalytic activity of micro-sized spherical Ag_3PO_4 particles was superior to the traditional visible-light active photocatalysts such as N-doped TiO_2 and $BiVO_4$ [11]. The research findings are considered as a breakthrough in the field of visible-light active photocatalysts [12]. Therefore, it is urgent to further investigate the basic principles and application of Ag_3PO_4 photocatalyst in detail. So far, various methods have been proposed to further enhance the photocatalytic activity of Ag_3PO_4 under visible light irradiation. One approach is the coupling of Ag_3PO_4 with other semiconductors or noble metals to promote the charge separation efficiency of Ag_3PO_4, and thus improving the

photocatalytic activity. Some coupled systems such as Ag_3PO_4/TiO_2 [13], Ag_3PO_4/AgX (X=Cl, Br, I) [14], Ag_3PO_4/SnO_2 [15], Fe_3O_4/Ag_3PO_4 [16], Ag_3PO_4/Ag [17, 18], Ag_3PO_4/BiOCl [19], Ag_3PO_4/reduced graphite oxide sheets [20], and carbon quantum dots/Ag_3PO_4 [21] composites have recently been developed to improve the photocatalytic activity of Ag_3PO_4. Another approach is the synthesis of Ag_3PO_4 with various new morphologies. This is because photocatalytic reactions are typically surface-based processes, thus the photocatalytic efficiency is closely related to the morphology and micro-structure of a photocatalyst [22]. Recently, research on Ag_3PO_4 crystals with new morphologies and structures has drawn a great deal of attention [23-31]. For examples, Bi et al. reported the single-crystalline Ag_3PO_4 rhombic dodecahedrons with only {110} facets exposed and cubes bounded entirely by {100} facets, and they found that both of these samples exhibited higher photocatalytic activity than the micro-sized spherical Ag_3PO_4 particles [23]. Wang et al. reported the synthesis of Ag_3PO_4 tetrapod microcrystals with exposed {110} facets, and they demonstrated that Ag_3PO_4 tetrapod showed higher photocatalytic activity than the micro-sized spherical Ag_3PO_4 particles [25]. Bi's group and Xie's group reported the synthesis of tetrahedral Ag_3PO_4 structures exposed with {111} planes, respectively [29, 30]. Our former work reported the synthesis of Ag_3PO_4 crystals with various new morphologies (branch, tetrapod, nanorod, triangular prism) by adjusting external experimental conditions [31]. However, it should be noted that the reported Ag_3PO_4 samples mostly possess regular crystal structures and exposed special planes. To the best of our knowledge, there is very little research on the

fabrication of mesocrystal Ag_3PO_4. Mesocrystals are colloidal crystals composed of individual nanocrystals that are aligned in a common crystallographic fashion, exhibiting scattering properties similar to a single crystal [32]. It is known that the mesocrystalline materials received significant research attentions because they simultaneously own both high porosity and high crystallinity [32-35], which is beneficial for photocatalytic application. Thus, the controlled synthesis of Ag_3PO_4 mesocrystals is of great value.

In this work, tetrahedral Ag_3PO_4 mesocrystals were synthesized by a new method. The effects of synthesis conditions on morphologies are investigated in detail, and the formation mechanism of tetrahedral Ag_3PO_4 mesocrystals is proposed. It is considered that the obtained tetrahedron could be formed through the oriented self-assembly of Ag_3PO_4 nanoparticles. More importantly, the as-prepared tetrahedral Ag_3PO_4 mesocrystals exhibit excellent photocatalytic activity under visible light irradiation for methylene blue (MB) and methyl orange (MO) removal.

2. Experimental

2.1 Sample preparation

In a typical preparation procedure for tetrahedral Ag_3PO_4 mesocrystals at optimized condition, firstly, 1.4 mL oleic acid was added into 9 mL of N,N-dimethylformamide (DMF) with stirring for 10 min to form transparent solution A. Then, 1 mmol of $AgNO_3$ was added into 1 mL of deionized water (H_2O) to form transparent solution B. The total volume of mixture solvent is kept constant to 10 mL. Subsequently, solution B was added into solution A under stirring. After stirring for 10 min, H_3PO_4 (3 mL, 85%) dissolved in

5 mL of ethanol was then added dropwise into the above solution under stirring. This process needs about 15 min. The mixture was stirred for 1 h and separated by centrifuge followed by washing with ethanol and deionized water for 3 times, respectively, to remove the oleic acid, DMF, and other residues. The product was then dried in a vacuum oven at 60 °C. Other samples were prepared by the similar procedure, except for different amount of oleic acid, P source, ratio of DMF to H_2O, and reaction temperature. For comparison purpose, micro-sized spherical Ag_3PO_4 particles were synthesized by a reported method [11].

2.2 Characterization

X-ray diffraction (XRD) experiments were carried out with a D/max-2400 diffractometer (Rigaku, Tokyo, Japan) using Cu-Ka radiation. The morphologies of the samples were examined by scanning electron microscopy (SEM; S-4800, Hitachi, Tokyo, Japan). A FEI Tecnai G2 F30 (Eindhoven, the Netherlands) transmission electron microscope, equipped with a Gatan imaging filter (GIF) system, was used for transmission electron microscopy (TEM), selected-area electron diffraction pattern (SAED), and energy dispersive X-ray spectra (EDX) work. Fourier transform infrared spectrum (FTIR) of the sample was recorded between 400 and 4000 cm^{-1} on a Nicolet NEXUS 670 FTIR spectrometer (Thermo-Nicolet, Madison, WI). Ultraviolet–visible diffuse reflectance spectra (UV–vis DRS) were measured using a Perkin Elmer 950 spectrometer (Perkin Elmer, Norwalk, CT), while $BaSO_4$ was used as a reference. Specific surface areas were computed from the isotherms by applying the

Brunauer–Emmett–Teller (BET) method using a Micromeritics ASAP 2000 system (Atlanta, GA).

2.3 Evaluation of photocatalytic activity

The photocatalytic activity of samples was measured by the decomposition of MB and MO in a reactor at room temperature. In a typical process for degradation of MB and MO, the used amount of photocatalyst was 0.02 g/70 mL of MB or MO solutions (10 mg/L). Before irradiation, the suspensions were stirred in the dark for 1 h to ensure the establishment of adsorption–desorption equilibrium. A 350 W Xe lamp with a cutoff filter of 420 nm was employed for the visible-light irradiation source and positioned 20 cm away from the reactor to trigger the photocatalytic reaction. A certain volume of suspension was withdrawn at selected times for analysis. After recovering the photocatalyst by centrifugation, the concentration of dye solution was analyzed by measuring the light absorption of the clear solution at 664 nm (λ_{max} for MB solution) or 465 nm (λ_{max} for MO solution) using a spectrophotometer (WFJ-7200, Unico, USA). The percentage of degradation was calculated by C/C_0. Here, C is the concentration of remaining dye solution at each irradiated time interval, while C_0 is the initial concentration.

To compare the photocatalytic stability of spherical Ag_3PO_4 particles and tetrahedral Ag_3PO_4 mesocrystals, the cycling runs in photocatalytic degradation of MB were checked. After one cycle, the photocatalyst was filtrated and washed thoroughly with deionized water, and then fresh MB solution (10 mg/L) was added to the photocatalyst to

begin the next cycling run. Four consecutive cycles were completed and each cycle lasted for 180 min.

3. Results and Discussion

3.1 Characterizations of tetrahedral Ag_3PO_4 mesocrystals

Based on the investigation of effects of synthesis conditions on the morphologies (see Fig. S1–S4 in the Supplementary Data), it is suggested that homogeneous tetrahedral Ag_3PO_4 could be synthesized under the optimized conditions: 1.4 ml of oleic acid as the surfactant, H_3PO_4 as the phosphorus (P) source, DMF/H_2O = 9:1, room temperature, and reaction time of 1 h. Low magnification SEM image (Fig. 1a) of the resulting Ag_3PO_4 synthesized at optimized condition shows that the product mainly consists of regularly shaped tetrahedrons (accounts for 85%). The average apex-to-apex length of these tetrahedrons is taken from statistics analysis, which is about 1.1 μm, as shown in Fig. 1b. A large magnification SEM image of as-prepared Ag_3PO_4 is displayed in Fig. 1c. It is noted that the surfaces of Ag_3PO_4 tetrahedrons are not smooth enough, which are covered by many nanoparticles. In addition, it is observed that some pores exist on the surfaces of Ag_3PO_4 tetrahedron (Fig. 1d), indicating the existence of surface porous characteristics. These observations suggest that the Ag_3PO_4 tetrahedron consists of nanoparticles.

Further investigation of Ag_3PO_4 tetrahedron was carried out by TEM technology, as shown in Fig. 2a. It exhibits a triangular morphology in two dimensions that could arise from a tetrahedral morphology in three dimensions. Moreover, it is observed that many nanoparticles are attached to the edges of Ag_3PO_4 tetrahedron, which is consistent with

the SEM result. Fig. 2b displays the SAED pattern of a single Ag_3PO_4 tetrahedron. The pattern consists of diffraction spots, revealing the single-crystalline nature of each Ag_3PO_4 tetrahedron. Generally, the mesoporous structure and the "single-crystal-like" diffraction are considered as the characterizations of mesocrystalline materials [36]. Combining the above results, it can be concluded that the as-prepared sample should be tetrahedral Ag_3PO_4 mesocrystals. Fig. 2c displays the EDX spectrum of tetrahedral Ag_3PO_4 sample. It reveals the O, P, and Ag peaks except for C and Cu peaks coming from the film on the TEM grid. This result clearly confirms the existence of the O, P and Ag elements.

The phase purity of as-obtained tetrahedral product was examined by means of XRD and FTIR methods. Fig. 3a clearly reveals that all of the diffraction peaks of the as-prepared tetrahedral sample can be indexed to the body-centered cubic structure of Ag_3PO_4 (JCPDS Card No. 06-0505). Moreover, the sharp diffraction peaks indicate high crystallinity of tetrahedral Ag_3PO_4 mesocrystals. In addition, it is noted that the intensity ratios of diffraction peaks are close to that of the standard values for powder sample, suggesting there is no obvious preferred orientation behavior. Fig. 3b shows the FTIR spectrum of tetrahedral Ag_3PO_4 sample. It reveals four major absorption bands: a strong and broad absorption around 3400 cm^{-1} and a sharp band at 1670 cm^{-1} are observed, which could be attributed to the stretching vibration of O–H and the bending vibration of H–O–H of water molecules, respectively. Two strong absorption bands are observed at 989 and 558 cm^{-1}, which can be assigned to the molecular vibrations of phosphate (PO_4^{3-})

[26, 37]. This result clearly confirms that there are no oleic acid and DMF molecules adsorbed on the surface of the as-obtained tetrahedral Ag_3PO_4 sample.

3.2 Formation mechanism of tetrahedral Ag_3PO_4 mesocrystals

Reaction time-dependent experiments were carried out to investigate the formation mechanism of tetrahedral Ag_3PO_4 mesocrystals. From Fig. 4a, it is obvious that the obtained samples prepared with various reaction times all show the cubic phase of Ag_3PO_4, and the crystallinity undergoes no obvious change when prolonging the reaction time. Reaction time-dependent morphological evolution is displayed in Fig. 4b–d. At the initial stage (0 min), nanoscale Ag_3PO_4 particles with size of about 100 nm are observed (Fig. 4b). As the reaction time increased to 30 min, besides the independent nanoparticles, tetrahedral morphology is observed (Fig. 4c). It can be seen that the tetrahedron consists of a large number of nanoparticles (marked with circles in Fig. 4c). When the reaction time was prolonged to 1 h, as shown in Fig. 4d, homogeneous and regular tetrahedrons were obtained, and the independent nanoparticles disappeared, implying that the tetrahedrons could be formed by an assembly process of nanoparticles. This result agrees well with the typical formation processes of mesocrystalline materials [32], further confirming the formation of tetrahedral Ag_3PO_4 mesocrystals.

From the characterization and time-dependent morphological evolution results, it is reasonable to presume that the tetrahedral Ag_3PO_4 mesocrystals were formed through the close-packed assembly of Ag_3PO_4 nanoparticles. This pathway is in stark contrast to the classical crystallization, which usually proceeds by molecule or ion-by-ion attachment

[36]. The formation of as-obtained tetrahedral Ag_3PO_4 mesocrystals could be based on the oriented aggregation mechanism, and the formation and evolution process can be divided into three steps: the initial formation of $[Ag(amide)(solvent)]^+$ ligand complex, the nucleation and growth processes, and the subsequent self-assembly process (oriented aggregation). A schematic diagram of the proposed formation process is shown in Scheme 1. In the first stage, the silver ions (Ag^+), amide (DMF), and solvent (H_2O) could form the weakly bound $[Ag(amide)(solvent)]^+$ ligand complex [38]. In addition, the oleic acid molecules could exist around the DMF instead of H_2O molecules due to its hydrophobic property. In this stage, the ratio of DMF to H_2O affects the resulting morphology. H_2O molecules could reduce the strength of the amide-silver ion binding energy, and excess amount of H_2O could induce the amide-silver ligand bond breaking [38], thus the role of oleic acid in the control of resulting morphology is limited because oleic acid molecules exist around the DMF instead of H_2O molecules. On the other hand, as displayed in Fig. S1 (in the Supplementary Data), oleic acid is essential for the formation of tetrahedral morphology. Hence, tetrahedral morphology disappears when the samples synthesized with low DMF/H_2O ratios (excess amount of H_2O), as shown in Fig. S2 (in the Supplementary Data). In the second stage, Ag_3PO_4 crystal nucleations were carried out after H_3PO_4 was added [31]. In this process, oleic acid molecules could adsorb on the surfaces of crystal nucleuses, which could control the reaction rate and avoid the crystallographic fusion of the primary crystals to a single crystal through the oriented-attachment mechanism [39]. These nucleation clusters were grown and then

transformed to crystalline primary Ag_3PO_4 nanoparticles (as building blocks) [40]. Thus, in a very short time, stabilized Ag_3PO_4 nanoparticles with surfactant coatings were formed. The obtained nanoparticles can be regarded as "spherical core-shell nanoparticles" with an inorganic core and an organic surfactant shell. It is known that the pH value affects the adsorption of surfactant molecules at the surface of inorganics, and thus influences the morphology of samples [41, 42]. Our experimental results (Fig. S3 in the Supplementary Data) confirmed that the acidic condition is beneficial for the formation of tetrahedral Ag_3PO_4 morphology, which could be due to the strong adsorption of oleic acid molecules on the surfaces of Ag_3PO_4 crystal nucleuses under acidic condition. In addition, the influence of reaction temperature on the adsorption of surfactant molecules at the surfaces of Ag_3PO_4 crystal nucleuses cannot be ignored in this stage. When the reaction was carried out at low temperature (e.g. 0 °C, shown in Fig. S4 in the Supplementary Data), the reactant diffusion decreased considerably and the adsorption of oleic acid molecules on the surfaces of Ag_3PO_4 crystal nucleuses became difficult, which led to the uncontrollable reaction process, thus forming the micro-sized spherical particles. In the third stage, tetrahedral Ag_3PO_4 mesocrystals were formed via a self-assembly process by aggregation of the building blocks (primary Ag_3PO_4 nanoparticles). When two building blocks with adsorbed surfactant oleic acid come together, the capillary forces between them facilitate the solvent removal and strengthen the agglomeration through van der Waals attractive forces [43, 44]. At this stage, the hydrophobic interactions between surfactant oleic acid molecules are regarded as the

driving force for the assembly. After self-assembly process, the surfactant oleic acid molecules were removed by washing in ethanol for several times. Due to the stacking defects and polydispersity of nanoparticles in the self-assembly process, some pores appeared on the surfaces of Ag_3PO_4 tetrahedron, as displayed in Fig. 1d. It is well-known that the detailed formation mechanism for self-assembly process is still largely unclear [36]. From our experimental results, it is confirmed that the ability of oleic acid is the driving force behind these polycrystalline tetrahedral assemblies. However, why the oleic acid induces the tetrahedral instead of other polyhedral assemblies is still unknown.

3.3 Optical absorption property and photocatalytic performance

For comparison purpose, micro-sized spherical Ag_3PO_4 particles were prepared by the reported method [11] (shown in Fig. S5 in the Supplementary Data). Then, the optical absorption properties of spherical Ag_3PO_4 particles and tetrahedral Ag_3PO_4 mesocrystals were compared, as shown in Fig. 5. Generally, the absorption edges of as-prepared samples are used to characterize their optical absorption properties, which could eliminate the influence of base absorption lines [31]. The absorption edge position was determined by the intersection of baseline with tangent line of the UV–vis absorption spectrum [24, 45, 46]. From Fig. 5, it is found that the spherical Ag_3PO_4 and tetrahedral Ag_3PO_4 mesocrystals posses the same absorption edge, which is around 525 nm.

The N_2 adsorption–desorption isotherms of spherical Ag_3PO_4 particles and tetrahedral Ag_3PO_4 mesocrystals are presented in Fig. 6. It can be seen that the areas of hysteresis loops for tetrahedral Ag_3PO_4 mesocrystals are much larger than that for

spherical Ag_3PO_4 particles, which indicates that much porous structures are presented in the sample of tetrahedral Ag_3PO_4 mesocrystals. The BET analysis shows that the specific surface areas of spherical Ag_3PO_4 and tetrahedral Ag_3PO_4 mesocrystals are 1.02 and 4.65 m^2/g, respectively. This result clearly indicates that tetrahedral Ag_3PO_4 mesocrystals exhibit higher BET surface area. The inset of Fig. 6 shows the corresponding pore size distributions of these two samples. It is observed that tetrahedral Ag_3PO_4 mesocrystals show a peak around 50 nm, which could be attributed to the pores on the surfaces of Ag_3PO_4 tetrahedron (as shown in Fig. 1d). On the contrary, there is no peaks of pore size distributions for the sample of spherical Ag_3PO_4 particles.

Before the photocatalytic reaction, the sample suspension was stirred for 1 h in the dark to reach the adsorption–desorption equilibrium. The adsorption–desorption equilibriums of MB and MO dyes are shown in Fig. S6 (in the Supplementary Data). It is found that the tetrahedral Ag_3PO_4 mesocrystals exhibit higher adsorption ability than spherical Ag_3PO_4, which is consistent with the BET specific surface areas of samples. Higher BET specific surface area of tetrahedral Ag_3PO_4 mesocrystals increases the adsorption of dye molecules. The photocatalytic behaviors of spherical Ag_3PO_4 and tetrahedral Ag_3PO_4 mesocrystals were explored for degradation of the positively charged MB and negatively charged MO molecules under visible light irradiation after the adsorption–desorption equilibriums, as shown in Fig. 7a–b. It should be pointed out that the self-degradation of MB and MO is slight, indicating the stabilization of these two dyes under visible light irradiation. For the degradation of MB, about 97% and 72% of

the initial MB molecules were decomposed by tetrahedral Ag_3PO_4 mesocrystals and spherical Ag_3PO_4 after photocatalytic reaction, respectively. Clearly, the photocatalytic degradation rate of tetrahedral Ag_3PO_4 mesocrystals is higher (25%) than that of spherical Ag_3PO_4 for the positively charged MB molecules. For the degradation of MO, about 92% of the initial MO molecules were decomposed for tetrahedral Ag_3PO_4 mesocrystals while 60% for spherical Ag_3PO_4 after photocatalytic reaction. This result indicates that tetrahedral Ag_3PO_4 mesocrystals show much higher (32%) photocatalytic degradation rate than spherical Ag_3PO_4 for the negatively charged MO molecules. Overall, the tetrahedral Ag_3PO_4 mesocrystals exhibit higher photocatalytic activity than spherical Ag_3PO_4 for degradation of MB and MO. The insets of Fig. 7a–b display the color changes of MB and MO solution during the photocatalytic degradation process corresponding to tetrahedral Ag_3PO_4 mesocrystals. It is clear that MB and MO solutions were almost decolorized completely after the photocatalytic reactions.

The kinetics of photocatalytic reactions can be described using a first order reaction for low concentration of dye (MB and MO) solutions [47, 48]:

$$\ln(C_0 / C) = kt \quad (1)$$

where C_0 and C are the initial concentration and remaining concentration of dye solution, respectively, k is the apparent reaction rate constant, and t is the irradiation time.

Fig. 7c–d displays the apparent rate constants (k, min^{-1}), which is determined from the slopes of $\ln(C_0/C)$ versus irradiation time. It can be seen that the apparent rate constants are 0.014 min^{-1} for tetrahedral Ag_3PO_4 mesocrystals and 0.008 min^{-1} for

spherical Ag_3PO_4 during the decomposition of MB. In comparison, the apparent rate constants are 0.0098 min^{-1} for tetrahedral Ag_3PO_4 mesocrystals and 0.0036 min^{-1} for spherical Ag_3PO_4 during the decomposition of MO. Remarkably, the photocatalytic rate constants of tetrahedral Ag_3PO_4 mesocrystals are 1.8 and 2.7 times of that of spherical Ag_3PO_4 for degradation of MB and MO dye solutions, respectively. The correlation coefficient (R^2) represents the correlation degree between practical photocatalytic reaction and linear fit. It is found that the R^2 values of as-prepared samples are above 0.9, suggesting the data fit the first kinetic model well.

The reason of higher photocatalytic activity for tetrahedral Ag_3PO_4 mesocrystals could be attributed to the mesocrystal structure. The tetrahedral Ag_3PO_4 mesocrystals simultaneously possess both porous characteristics and high crystallinity. On one hand, the porous characteristics of tetrahedral Ag_3PO_4 mesocrystals contribute to a higher BET specific surface area. Since photocatalytic reactions are typically surface-based processes, the photocatalytic efficiency is closely related to the adsorption property of dyes on the surfaces of photocatalysts. The stronger the adsorption of dyes on the photocatalyst surface, the easier and faster the photocatalytic process [22]. The higher BET specific surface area of tetrahedral Ag_3PO_4 mesocrystals facilitates the adsorption of dye molecules, as shown in Fig. S6, which contributed to the higher photocatalytic activity. On the other hand, the tetrahedral Ag_3PO_4 mesocrystals display higher crystallinity compared with spherical Ag_3PO_4 sample, as shown in Fig. S7 (in the Supplementary Data). The well-crystallized phase of tetrahedral Ag_3PO_4 mesocrystals could facilitate the

transfer of photoinduced electrons during photocatalytic reactions, which decreased the probability of recombination with photoinduced holes and thus enhanced the efficiency of photocatalysis [49]. In addition, the optical absorption property is generally considered as an important factor affecting photocatalytic activity. However, it is found that the as-prepared spherical and tetrahedral Ag_3PO_4 products reveal the same absorption edge (shown in Fig. 5), implying that the light absorption property is not the major factor affecting photocatalytic activity.

Fig. 8 shows the photocatalytic stability of tetrahedral Ag_3PO_4 mesocrystals and spherical Ag_3PO_4 particles. It is observed that the photocatalytic activity of tetrahedral Ag_3PO_4 mesocrystals is decreased slowly in four successive experimental runs. However, the rate of MB degradation for spherical Ag_3PO_4 particles decreases more significantly in four successive experimental runs under the same conditions. This result indicates that the photocatalytic activity of tetrahedral Ag_3PO_4 mesocrystals is more stable compared with that of spherical Ag_3PO_4 particles.

4. Conclusion

Tetrahedral Ag_3PO_4 mesocrystals were firstly synthesized by a novel one-step chemical precipitation approach in the mixture solvent of DMF and H_2O using oleic acid as the surfactant. The homogeneous tetrahedral Ag_3PO_4 mesocrystals could be synthesized under optimized conditions. The as-prepared tetrahedral Ag_3PO_4 mesocrystals could be formed through the close-packed assembly of Ag_3PO_4 nanoparticles based on the oriented aggregation mechanism. Oleic acid is considered as

the aggregation-orienting agent for the formation of this unique Ag_3PO_4 tetrahedron. Furthermore, the photocatalytic rate constants of tetrahedral Ag_3PO_4 mesocrystals are 1.8 and 2.7 times of that of spherical Ag_3PO_4 for degradation of MB and MO dye solutions, respectively. Overall, this work shows that it is possible to design and synthesize mesocrystalline materials by a simple oleic acid-mediated approach in the mixture solvent.

Acknowledgements

This work is financially supported by the National Natural Science Foundation of China (Grant No. 21403184), Natural Science Foundation of the Jiangsu Higher Education Institutions of China (Grant No. 14KJB150025), National Key Technology R&D Program of China (Grant No. 2013BAC13B01), and National Natural Science Foundation of China (No. 21276220).

References

[1] M.R. Hoffmann, S.T. Martin, W. Choi, D.W. Bahnemann, Chem. Rev. 95 (1995) 69-96.

[2] A. Fujishima, K. Honda, Nature 238 (1972) 37-38.

[3] C.H. Cho, D.K. Kim, D.H. Kim, J. Am. Ceram. Soc. 86 (2003) 1138-1145.

[4] R. Asahi, T. Morikawa, T. Ohwaki, K. Aoki, Y. Taga, Science 293 (2001) 269-271.

[5] G. Chen, Y. Wang, J. Zhang, C. Wu, H. Liang, H. Yang, J. Nanosci. Nanotechnol. 12 (2012) 3799-3805.

[6] P. Dong, Y. Wang, L. Guo, B. Liu, S. Xin, J. Zhang, Y. Shi, W. Zeng, S. Yin, Nanoscale 4 (2012) 4641-4649.

[7] Y. Wang, G. Chen, Q. Shen, F. Zhang, G. Chen, Mater. Lett. 116 (2014) 27-30.

[8] G. Chen, Y. Wang, F. Zhang, H. Liang, F. Wang, L. Li, J. Sol-Gel Sci. Technol. 64 (2012) 564-570.

[9] P. Dong, B. Liu, Y. Wang, H. Pei, S. Yin, J. Mater. Res. 25 (2010) 2392.

[10] Y. Wang, G. Chen, Q. Shen, H. Yang, L. Li, Y. Song, J. Nanosci. Nanotechnol. 14 (2014) 4988-4994.

[11] Z. Yi, J. Ye, N. Kikugawa, T. Kako, S. Ouyang, H. Stuart-Williams, H. Yang, J. Cao, W. Luo, Z. Li, Nat. Mater. 9 (2010) 559-564.

[12] C.T. Dinh, T.D. Nguyen, F. Kleitz, T.O. Do, Chem. Commun. 47 (2011) 7797-7799.

[13] W. Yao, B. Zhang, C. Huang, C. Ma, X. Song, Q. Xu, J. Mater. Chem. 22 (2012) 4050–4055.

[14] Y. Bi, S. Ouyang, J. Cao, J. Ye, Phys. Chem. Chem. Phys. 13 (2011) 10071-10075.

[15] L. Zhang, H. Zhang, H. Huang, New J. Chem. 36 (2012) 1541–1544.

[16] G. Li, L. Mao, RSC Adv. 2 (2012) 5108–5111.

[17] Y. Bi, H. Hu, S. Ouyang, Z. Jiao, G. Lu, J. Ye, J. Mater. Chem. 22 (2012) 14847-14850.

[18] Y. Bi, H. Hu, S. Ouyang, Z. Jiao, G. Lu, J. Ye, Chem. Eur. J. 18 (2012) 14272-14275.

[19] B. Cao, P. Dong, S. Cao, Y. Wang, J. Am. Ceram. Soc. 96 (2013) 544-548.

[20] P. Dong, Y. Wang, B. Cao, S. Xin, L. Guo, J. Zhang, F. Li, Appl. Catal., B 132-133 (2013) 45-53.

[21] H. Zhang, H. Huang, H. Ming, L. Zhang, J. Mater. Chem. 22 (2012) 10501-10506.

[22] H. Tong, S. Ouyang, Y. Bi, N. Umezawa, M. Oshikiri, J. Ye, Adv. Mater. 24 (2012) 229-251.

[23] Y. Bi, S. Ouyang, N. Umezawa, J. Cao, J. Ye, J. Am. Chem. Soc. 133 (2011) 6490-6492.

[24] W. Jun, F. Teng, M. Chen, CrystEngComm 15 (2013) 39-42.

[25] H. Wang, L. He, L. Wang, P. Hu, L. Guo, X. Han, J. Li, CrystEngComm 14 (2012) 8342–8344.

[26] Q. Liang, W. Ma, Y. Shi, Z. Li, X. Yang, CrystEngComm 14 (2012) 2966-2973.

[27] Y. Bi, H. Hu, Z. Jiao, H. Yu, G. Lu, J. Ye, Phys. Chem. Chem. Phys. 14 (2012) 14486-14488.

[28] Z. Jiao, Y. Zhang, H. Yu, G. Lu, J. Ye, Y. Bi, Chem. Commun. 49 (2013) 636-638.

[29] H. Hu, Z. Jiao, H. Yu, G. Lu, J. Ye, Y. Bi, J. Mater. Chem. A 1 (2013) 2387-2390.

[30] B. Zheng, X. Wang, C. Liu, K. Tan, Z. Xie, L. Zheng, J. Mater. Chem. A 1 (2013) 12635-12640.

[31] P. Dong, Y. Wang, H. Li, H. Li, X. Ma, L. Han, J. Mater. Chem. A 1 (2013) 4651-4656.

[32] M. Niederberger, H. Colfen, Phys. Chem. Chem. Phys. 8 (2006) 3271-3287.

[33] L. Li, C.-y. Liu, CrystEngComm 12 (2010) 2073-2078.

[34] Y. Aoyama, Y. Oaki, R. Ise, H. Imai, CrystEngComm 14 (2012) 1405-1411.

[35] Z. Hong, M. Wei, T. Lan, L. Jiang, G. Cao, Energy Environ. Sci. 5 (2012) 5408-5413.

[36] H. Cölfen, M. Antonietti, Angew. Chem. Int. Ed. 44 (2005) 5576-5591.

[37] M. Thomas, S.K. Ghosh, K.C. George, Mater. Lett. 56 (2002) 386-392.

[38] V. Romanov, C.-K. Siu, U.H. Verkerk, A.C. Hopkinson, K.W.M. Siu, J. Phys. Chem. A 114 (2010) 6964-6971.

[39] Q. Gong, X. Qian, X. Ma, Z. Zhu, Cryst. Growth Des. 6 (2006) 1821-1825.

[40] H. Cölfen, S. Mann, Angew. Chem. Int. Ed. 42 (2003) 2350-2365.

[41] J. Drelich, Y. Lu, L. Chen, J.D. Miller, S. Guruswamy, Appl. Surf. Sci. 125 (1998) 236-244.

[42] L. Qi, H. Cölfen, M. Antonietti, Chem. Mater. 12 (2000) 2392-2403.

[43] V.N. Manoharan, D.J. Pine, MRS Bull. 29 (2004) 91-95.

[44] V.N.T.K. Satyanarayana, S.K. Ajay, S. Sudipta, Nanotechnology 18 (2007) 075303.

[45] A. Wolberg, J.F. Roth, J. Catal. 15 (1969) 250-255.

[46] C.-F. Chi, H.-W. Cho, H. Teng, C.-Y. Chuang, Y.-M. Chang, Y.-J. Hsu, Y.-L. Lee, Appl. Phys. Lett. 98 (2011) 012101-012101-012103.

[47] J.M. Herrmann, H. Tahiri, Y. Ait-Ichou, G. Lassaletta, A. Gonzalez-Elipe, A. Fernandez, Appl. Catal., B 13 (1997) 219-228.

[48] X.H. Wang, J.G. Li, H. Kamiyama, Y. Moriyoshi, T. Ishigaki, J. Phys. Chem. B 110 (2006) 6804-6809.

[49] H. Li, J. Li, Y. Huo, J. Phys. Chem. B 110 (2006) 1559-1565.

Figure captions:

Fig. 1. (a) SEM image of Ag_3PO_4 tetrahedron synthesized at optimized condition: 1.4 mL oleic acid, H_3PO_4, DMF/H_2O = 9:1, 25°C, 1 h; (b) the apex-to-apex length distribution of these tetrahedrons; and (c–d) Ag_3PO_4 tetrahedron at large magnifications.

Fig. 2. (a) TEM image of Ag_3PO_4 tetrahedron synthesized at optimized condition, the inset is a typical Ag_3PO_4 tetrahedron; (b) SAED pattern of a single Ag_3PO_4 tetrahedron; and (c) EDX spectrum of Ag_3PO_4 tetrahedron.

Fig. 3. XRD pattern (a) and FTIR spectrum (b) of the as-prepared tetrahedral sample.

Fig. 4. XRD patterns (a) and SEM images (b–d) of Ag_3PO_4 products prepared with various reaction times: (b) 0 min, (c) 30 min, and (d) 1 h. (1.4 mL oleic acid, H_3PO_4, DMF/H_2O = 9:1, 25 °C)

Fig. 5. UV–vis absorption spectra of spherical Ag_3PO_4 and tetrahedral Ag_3PO_4 mesocrystals.

Fig. 6. N_2 adsorption-desorption isotherms for spherical Ag_3PO_4 particles and tetrahedral Ag_3PO_4 mesocrystals. The inset is the BJH pore size distributions from N_2 desorption branch.

Fig. 7. Variation of MB (a) and MO (b) concentration against irradiation time in the presence of spherical Ag_3PO_4, tetrahedral Ag_3PO_4 mesocrystals and without photocatalyst in the dark and under visible light irradiation (the insets shows the color changes of MB

and MO solution during the photocatalytic degradation process corresponding to the tetrahedral Ag_3PO_4 mesocrystals); plots of ln(C_0/C) versus irradiation time for MB (c) and MO (d) representing the fit using a pseudo-first-order reaction rate.

Fig. 8. Repeated photocatalytic degradation of MB solution in the presence of spherical Ag_3PO_4 particles and tetrahedral Ag_3PO_4 mesocrystals under visible light irradiation.

Scheme caption:

Scheme 1. Schematic illustration of the formation of tetrahedral Ag_3PO_4 mesocrystals.

Dear Rick Ubic, PhD,

We would like to submit the revised manuscript entitled “Facile synthesis of tetrahedral Ag_3PO_4 mesocrystals and its enhanced photocatalytic activity” (ID: MRB-14-148). These comments are valuable and helpful for revising and improving our article. We have carefully checked and revised the article as the requirements. Detailed revision is shown in revised manuscript in BOLD font.

All authors have approved the final submitted manuscript. Neither the entire paper nor any part of its content has been published or accepted elsewhere. It is not being submitted to any other journal. We confirm that this manuscript is original.

Yours sincerely,

Pengyu Dong* et al.

Dear Reviewers,

Thank you for the comments concerning our manuscript entitled “Facile synthesis of tetrahedral Ag_3PO_4 mesocrystals and its enhanced photocatalytic activity” (ID: MRB-14-148). These comments are valuable and helpful for revising and improving our article. We have carefully checked and revised the article as the requirements. Detailed revision is shown in revised manuscript in BOLD font.

Responds to the Reviewers' comments:

Reviewers' comments:

Reviewer #1: In this manuscript, authors prepared tetrahedral Ag_3PO_4 mesocrystals by a one-step chemical precipitation method, and investigated the formation mechanism as well as photocatalytic activities. This work is novel and interesting. I believe the authors did a high-quality job on optimizing the synthesis condition, analyzing the formation mechanism and evaluating the photocatalytic activities. Therefore, I would like to recommend it for publication after minor revisions addressed as following:

(1)Introduction, the statement "we used a new approach to prepare the tetrahedral Ag_3PO_4 mesocrystals", should be rewritten.

>**Response:** According to your good instruction, we rewrote this sentence as "tetrahedral Ag_3PO_4 mesocrystals were synthesized by a new method" in the revised manuscript.

(2) In 3.2 section, the sentence" some pores could be produced on the surfaces of Ag_3PO_4 tetrahedron" needs revision.

>**Response:** According to your good instruction, we rewrote this sentence as "some pores appeared on the surfaces of Ag_3PO_4 tetrahedron" in the revised manuscript.

(3) In 3.2 section, the authors write "It is known that H_2O molecules could reduce the strength of the amide-silver ion binding energy, and excess amount of H_2O could induce the amide-silver ligand bond breaking [38]. " I believe that " It is known" should be deleted, but the later sentence should be reserved.

>**Response:** According to your good instruction, "It is known that" was deleted in this sentence.

Reviewer 2:

This paper introduced the preparation of tetrahedral Ag_3PO_4 mesocrystals using an oleic acid assistant method. It is interest to find that the prepared Ag_3PO_4 mesocrystals exhibit enhanced visible-light photocatalytic activity compared to the micro-sized spherical Ag_3PO_4 particles. The paper is suggested to be published after considering the followed questions:

1. The mesocrystalline materials received significant research attentions because they simultaneously own both high porosity and high crystallinity. A comparison of the pore distribution in the tetrahedral Ag_3PO_4 mesocrystals and in micro-sized spherical Ag_3PO_4 particles should be given.

>**Response:** According to your good instruction, the N_2 adsorption–desorption isotherms of spherical Ag_3PO_4 particles and tetrahedral Ag_3PO_4 mesocrystals were measured, as shown in Fig. 6 (named Fig. 6 in the revised manuscript). It can be seen

that the areas of hysteresis loops for tetrahedral Ag_3PO_4 mesocrystals are much larger than that for spherical Ag_3PO_4 particles, which indicates that much porous structures are presented in the sample of tetrahedral Ag_3PO_4 mesocrystals. The BET analysis shows that the specific surface areas of spherical Ag_3PO_4 and tetrahedral Ag_3PO_4 mesocrystals are 1.02 and 4.65 m^2/g, respectively. This result clearly indicates that tetrahedral Ag_3PO_4 mesocrystals exhibit higher BET surface area. The inset of Fig. 6 shows the corresponding pore size distributions of these two samples. It is observed that tetrahedral Ag_3PO_4 mesocrystals show a peak around 50 nm, which could be attributed to the pores on the surfaces of Ag_3PO_4 tetrahedron (as shown in Fig. 1d). On the contrary, there is no peaks of pore size distributions for the sample of spherical Ag_3PO_4 particles.

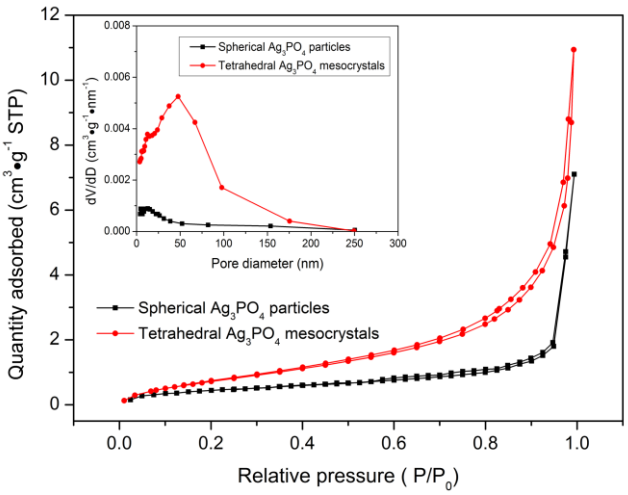

Fig. 6. N_2 adsorption-desorption isotherms for spherical Ag_3PO_4 particles and tetrahedral Ag_3PO_4 mesocrystals. The inset is the BJH pore size distributions from N_2 desorption branch.

2. The long-term stability of the photocatalytic activity of the tetrahedral Ag_3PO_4 mesocrystals should be checked.

>Response: According to your good instruction, the long-term stability of the photocatalytic activity of the tetrahedral Ag_3PO_4 mesocrystals and spherical Ag_3PO_4 particles was checked, as shown in Fig. 8 (named Fig. 8 in the revised manuscript).

In the Experimental section, it was described as "To compare the photocatalytic stability of spherical Ag_3PO_4 particles and tetrahedral Ag_3PO_4 mesocrystals, the cycling runs in photocatalytic degradation of MB were checked. After one cycle, the photocatalyst was filtrated and washed thoroughly with deionized water, and then fresh MB solution (10 mg/L) was added to the photocatalyst to begin the next cycling run. Four consecutive cycles were completed and each cycle lasted for 180 min."

In Results and Discussion section, it was described as "Fig. 8 shows the photocatalytic stability of tetrahedral Ag_3PO_4 mesocrystals and spherical Ag_3PO_4 particles. It is observed that the photocatalytic activity of tetrahedral Ag_3PO_4 mesocrystals is decreased slowly in four successive experimental runs. However, the rate of MB degradation for spherical Ag_3PO_4 particles decreases more significantly in four successive experimental runs under the same conditions. This result indicates that the photocatalytic activity of tetrahedral Ag_3PO_4 mesocrystals is more stable compared with that of spherical Ag_3PO_4 particles."

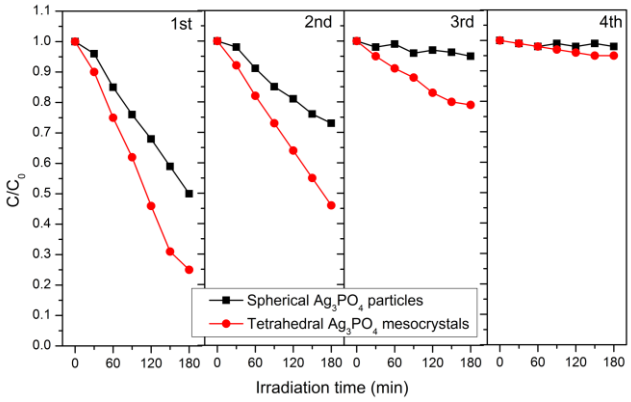

Fig. 8. Repeated photocatalytic degradation of MB solution in the presence of spherical Ag_3PO_4 particles and tetrahedral Ag_3PO_4 mesocrystals under visible light irradiation.

Materials Research Bulletin (MRB) New Manuscript Checklist

All new manuscripts should have the following:

- [Y] Text no smaller than 12 point type, double-spacing of all text pages including the references.
- [Y] Page numbers on each page.
- [Y] High quality figures, i.e. no photocopies of photographic plates, laser prints are acceptable.
- [Y] Large symbols used in figures, good enough for reproduction.
- [Y] Tables and figures at the end of the manuscript (no embedded tables/figures in text).
- [Y] Correct order:

-Abstract
-Introduction
-Experimental
-Results
-Discussion
-Conclusions
-References
-Tables (one table per 8½ X 11 page)
-Figure captions page
-Figures, with figure number, no caption (one figure per 8½ X 11 page)

Graphical Abstract (for review)

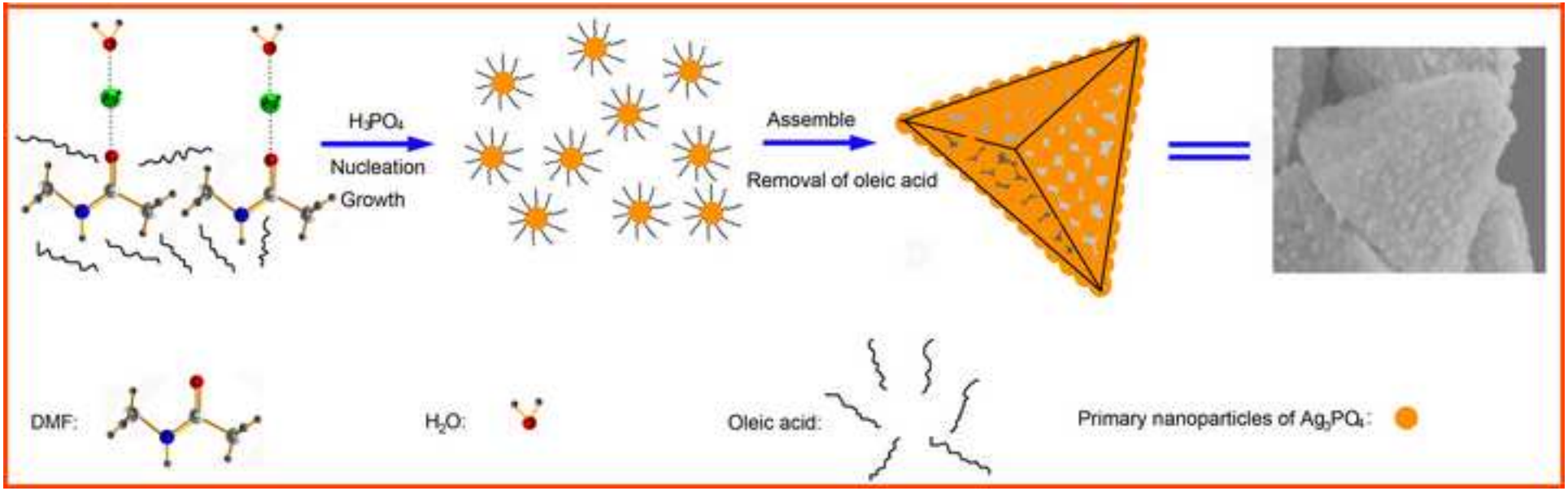

Highlights (for review)

> Tetrahedral Ag_3PO_4 mesocrystals were firstly synthesized.

> The formation mechanism of tetrahedral Ag_3PO_4 mesocrystals is proposed.

> The obtained tetrahedral Ag_3PO_4 mesocrystals exhibit larger BET surface area.

> The tetrahedral Ag_3PO_4 mesocrystals show enhanced photocatalytic activity.

Figure 1

Click here to download high resolution image

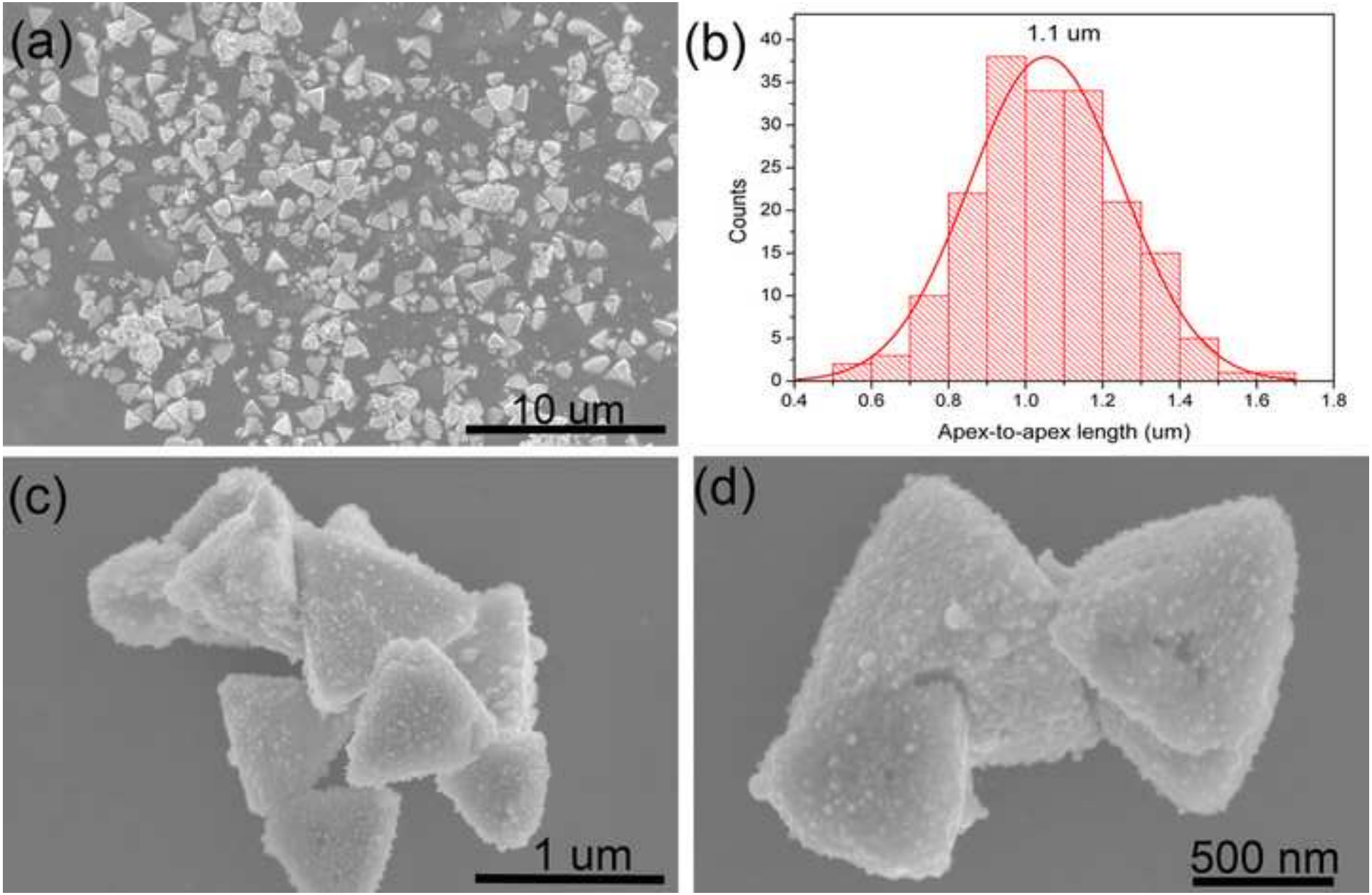

Figure 2

Click here to download high resolution image

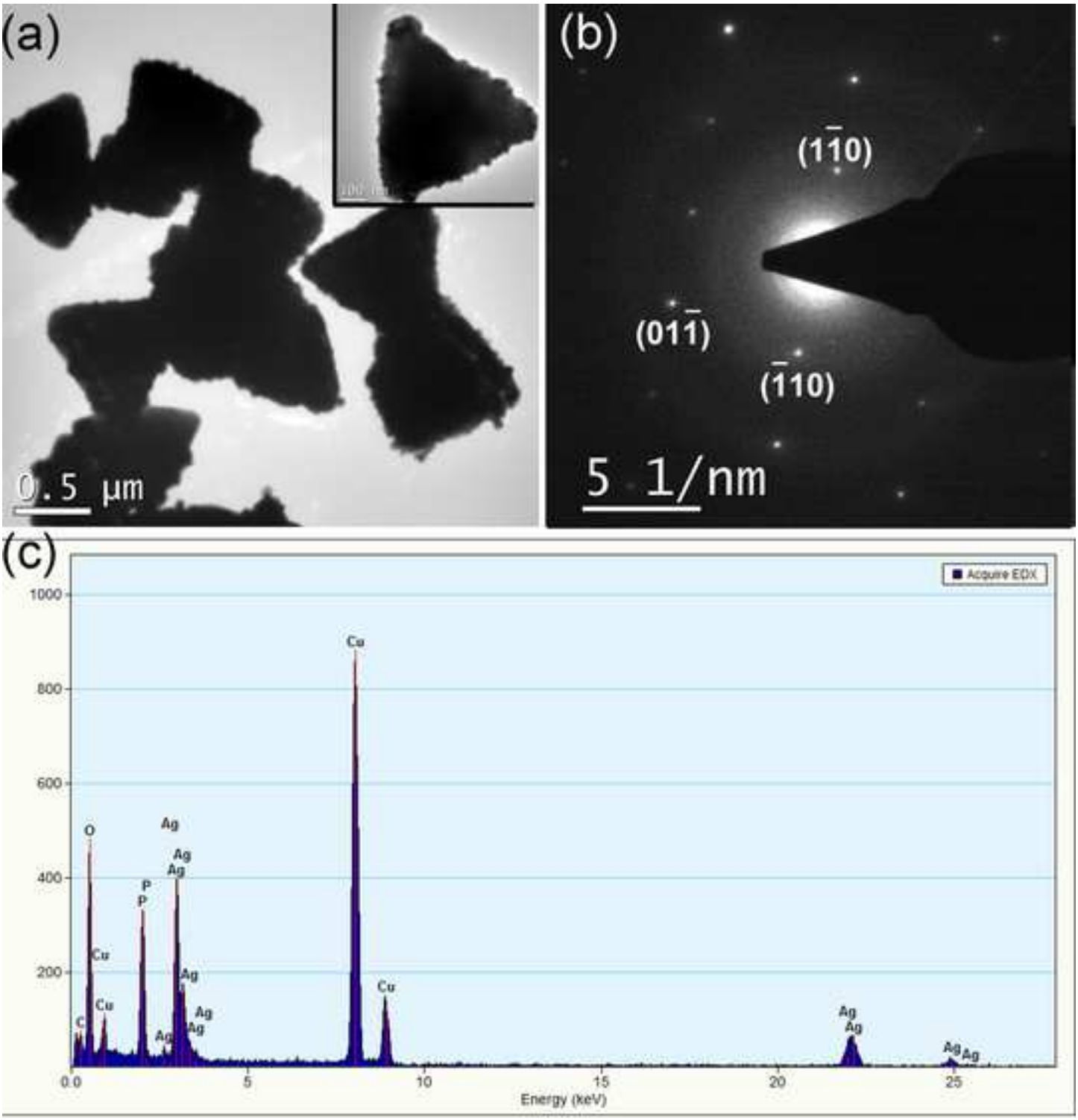

Figure 3
Click here to download high resolution image

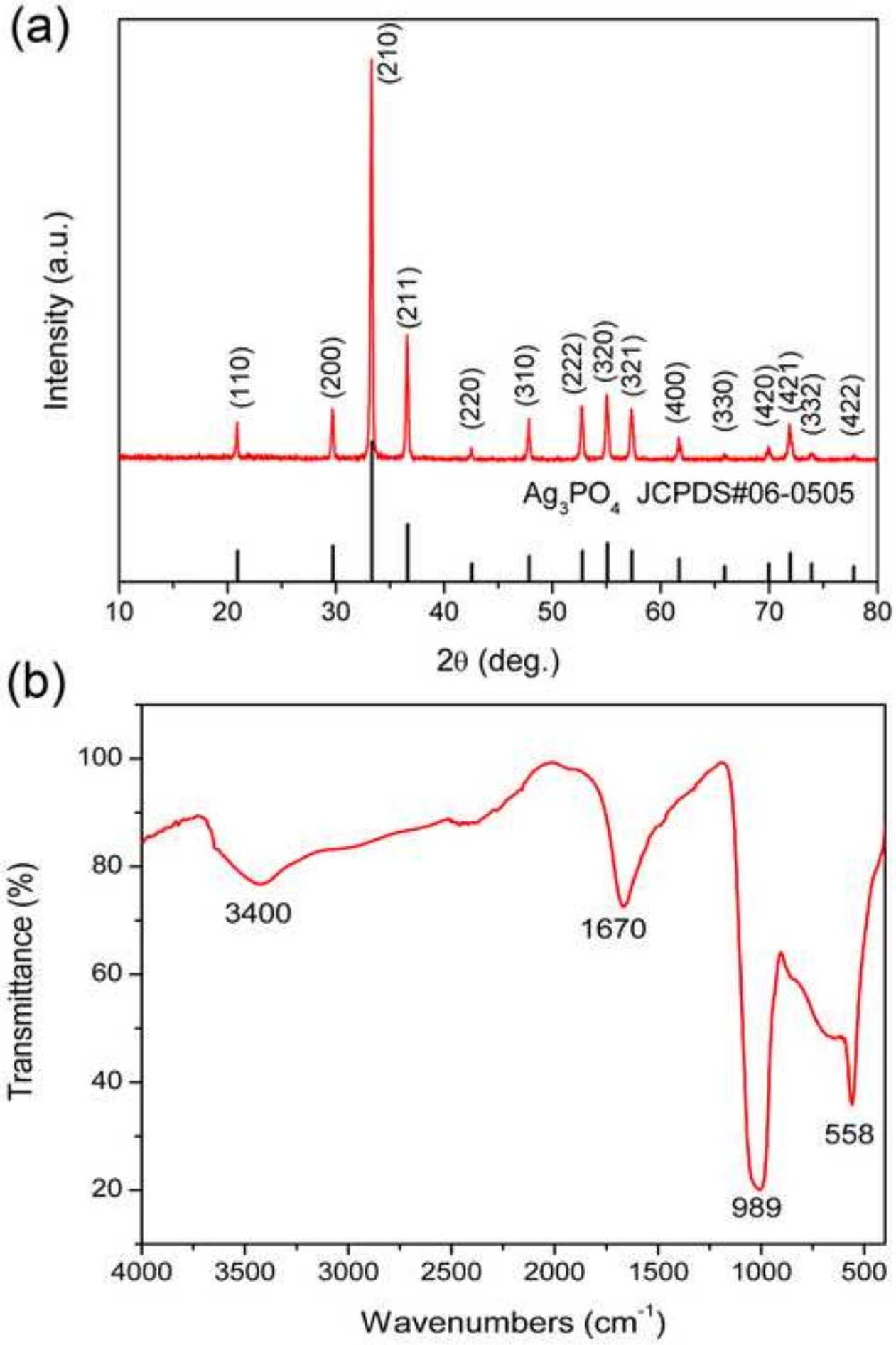

Figure 4

Click here to download high resolution image

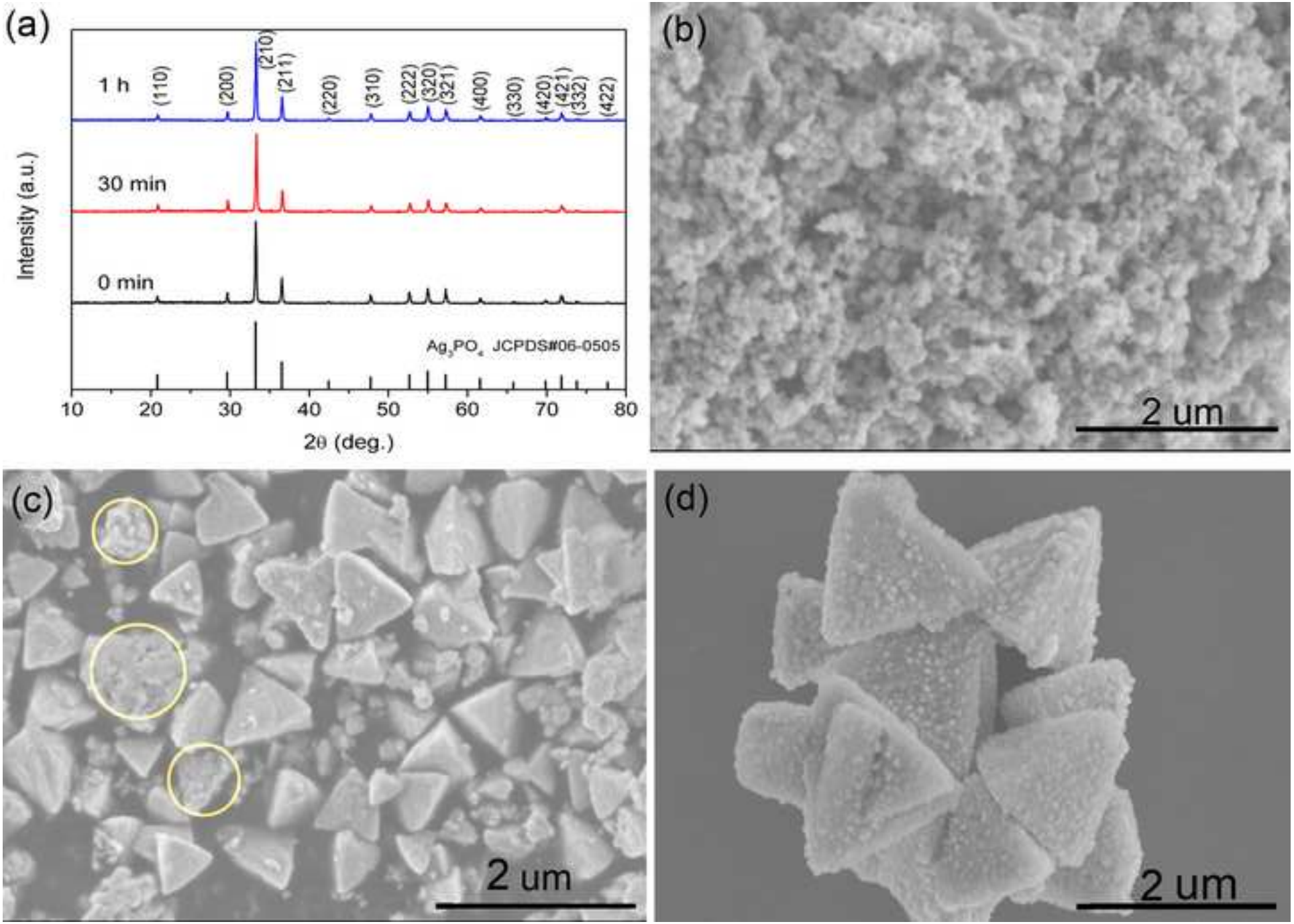

Figure 5

Click here to download high resolution image

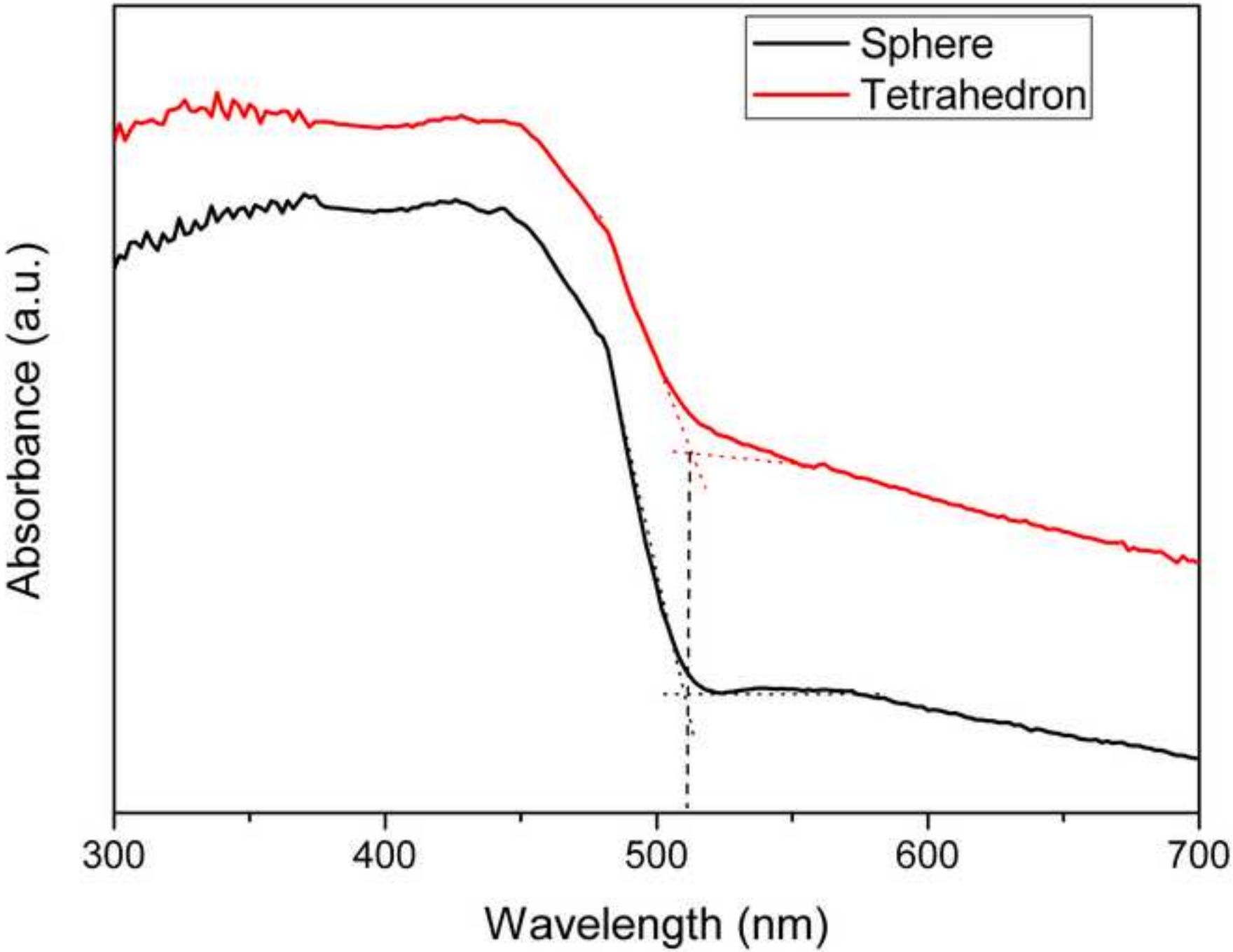

Figure 6

Click here to download high resolution image

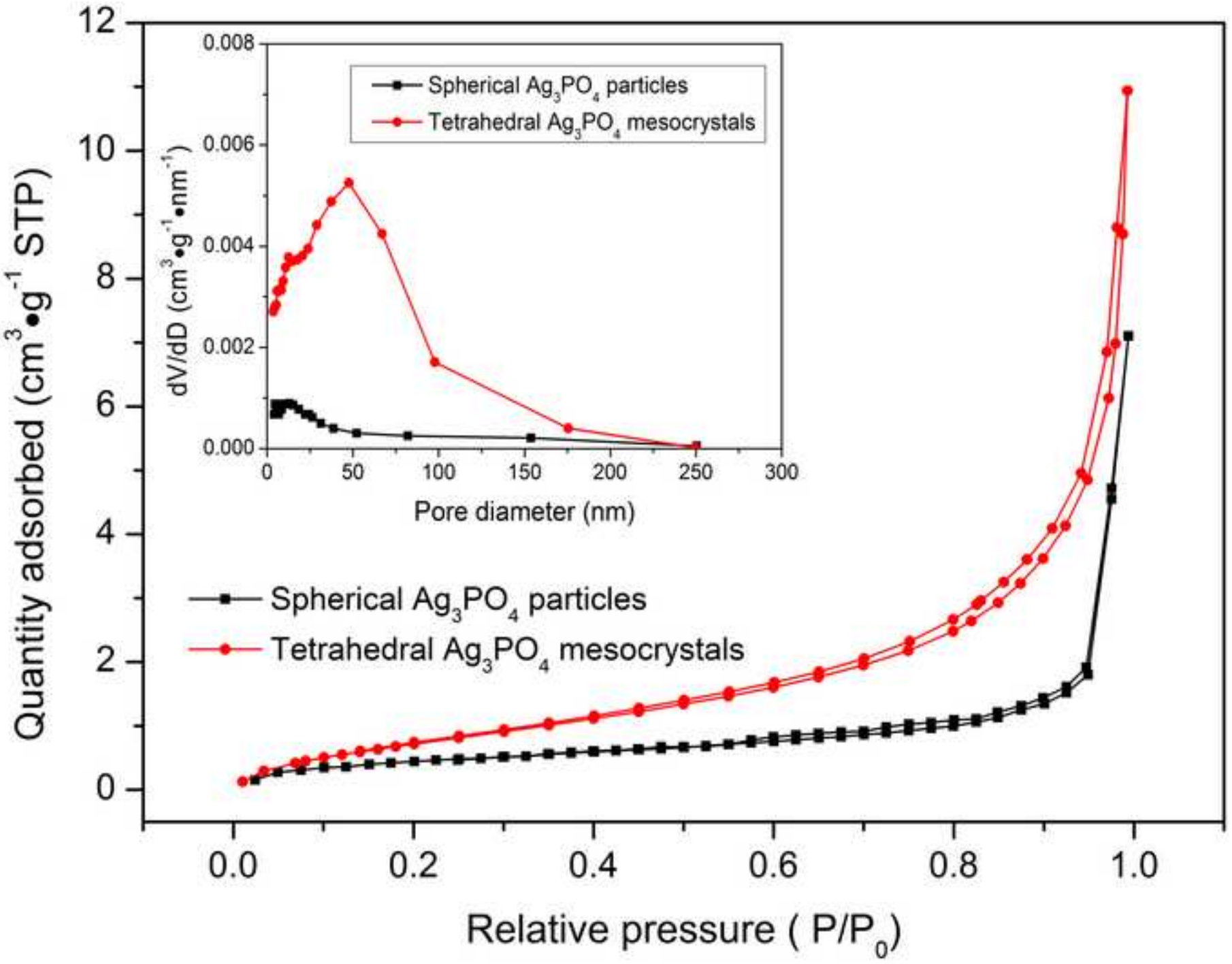

Figure 7

Click here to download high resolution image

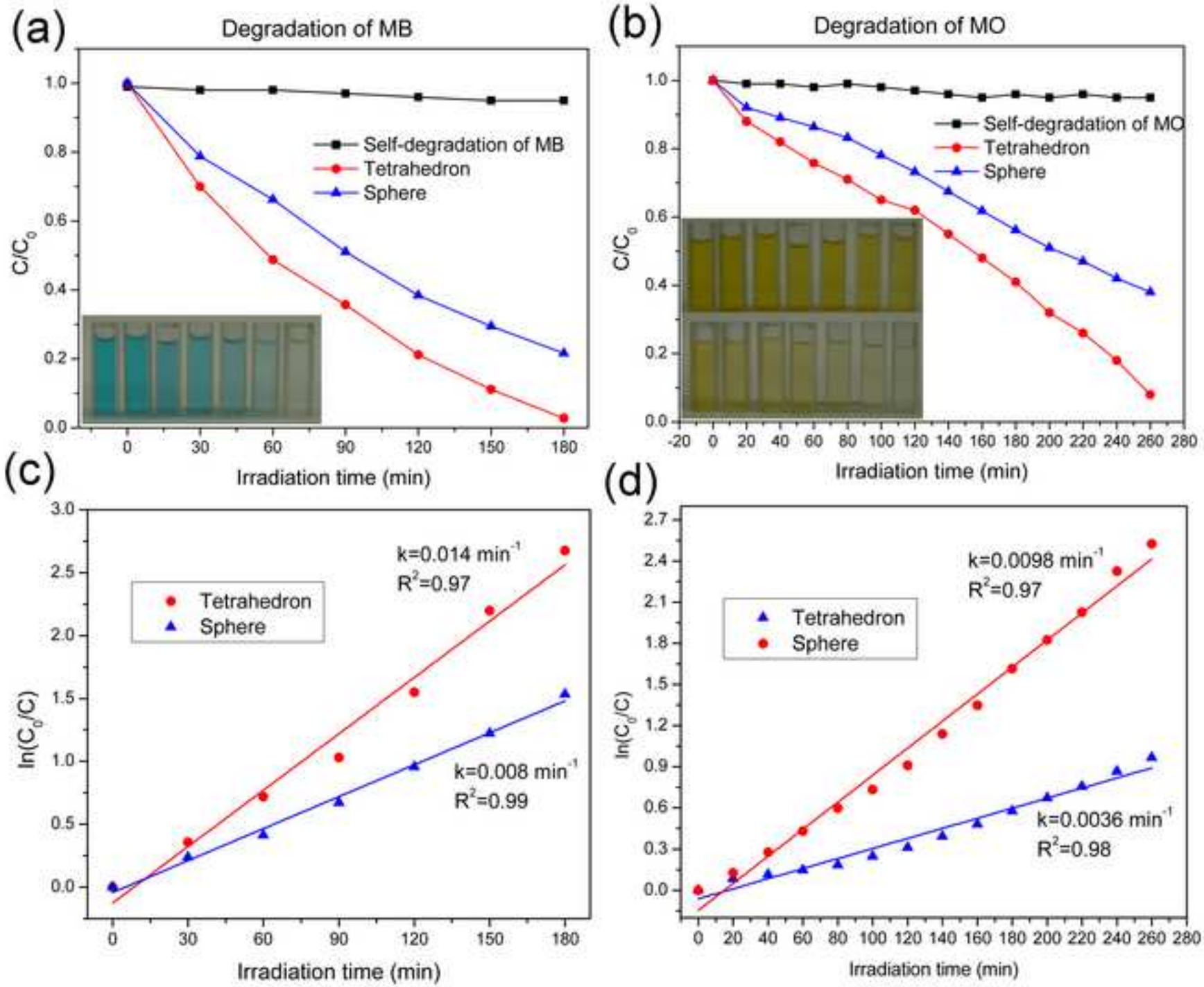

Figure 8

Click here to download high resolution image

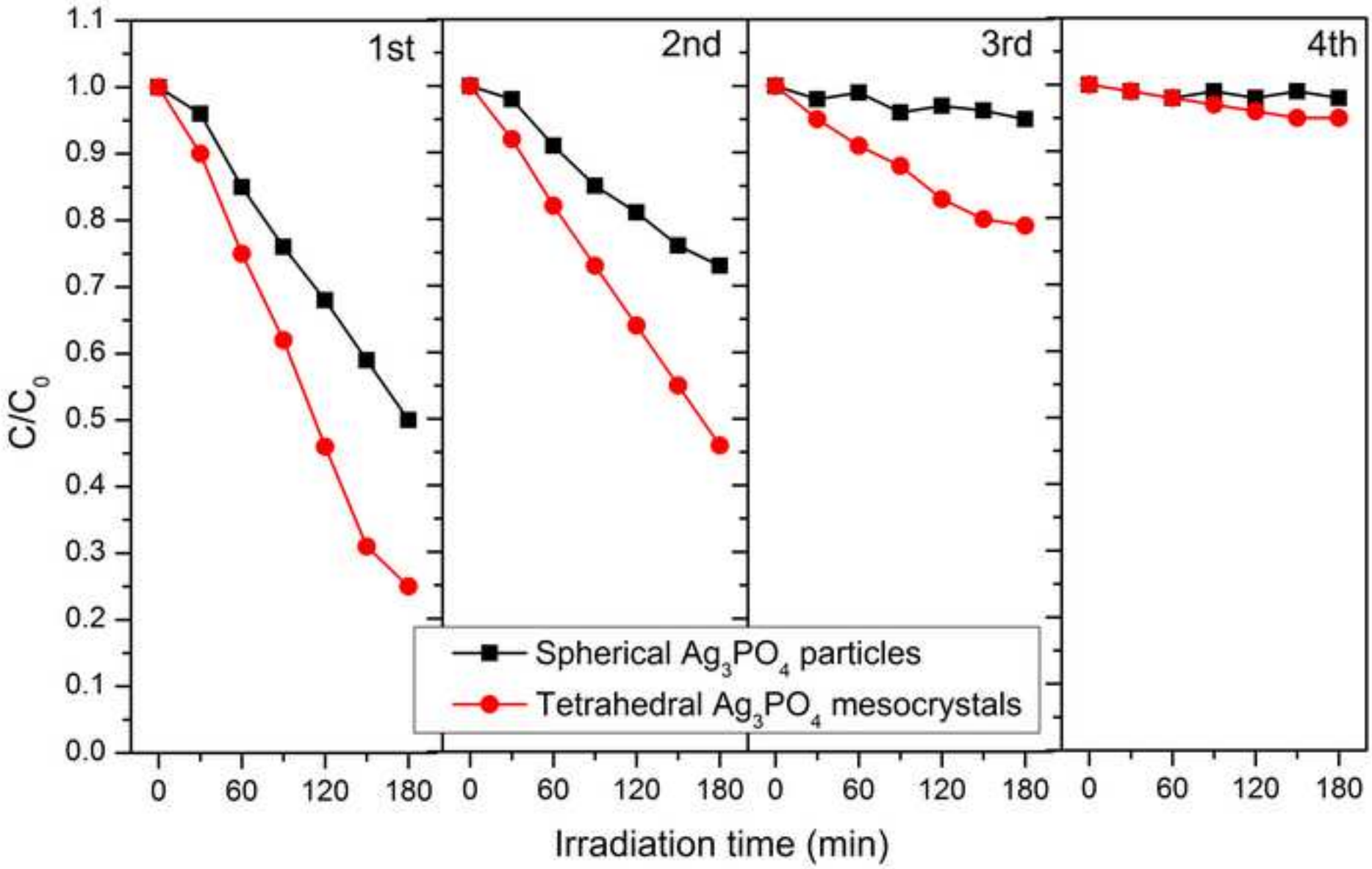

Scheme 1

Click here to download high resolution image

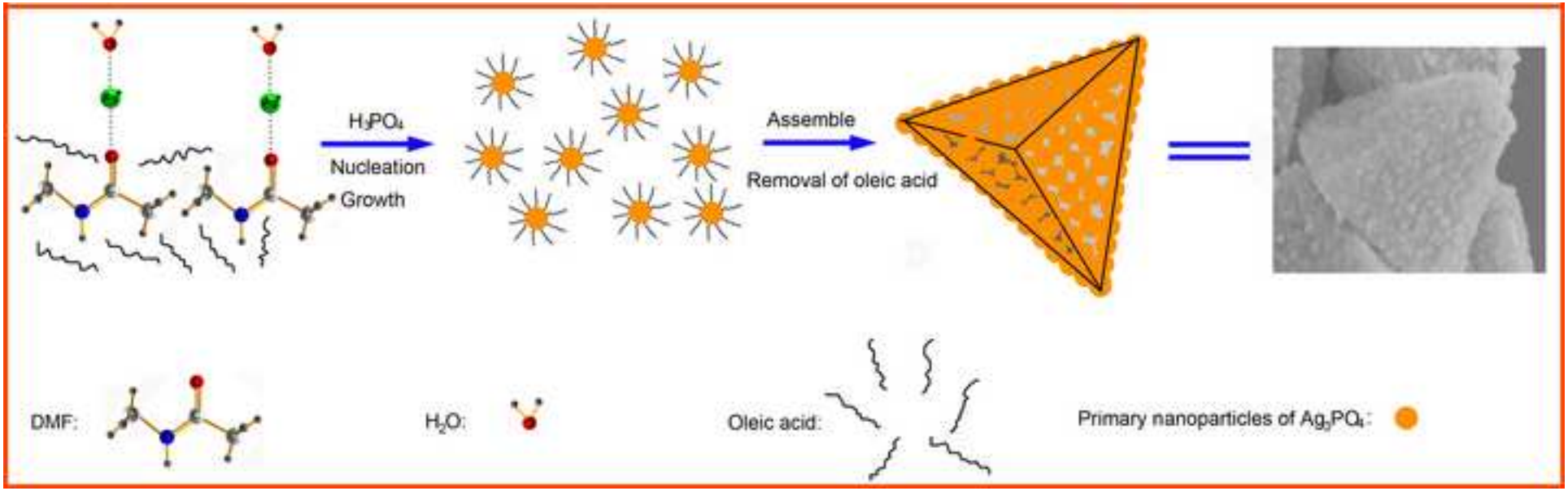

Supplementary Material

Click here to download Supplementary Material: Supplementary Data.doc